

# Wonders of the Atmosphere Chapter 11: Halos

Started 08 Mar 2025

### 11.1 Halos, Overlooked Cousins of Rainbows

Outside the polar regions or ski slopes, halos are the overlooked cousins of rainbows. Produced when ice crystals refract and/or reflect sunlight, they often form beautiful rings, arcs, or spots of light in the sky above entire unseeing populations. There are times, though that you are immersed in such a bewildering array of brilliant halos, as in Fig. 11-1, you can't help being awestruck, as Jack London was when he saw diamond dust in the Klondike gold-rush Alaska.

It is clear and cold....And in the sky are three suns, and all the air is flashing with the dust of diamonds. *The Sundog Trail*,

Two of these 'Suns' are not Suns at all, but brilliant halo spots directly right and left of the Sun called *parhelia*, mock Suns, or Sun dogs (because they 'follow their master', the Sun), (Fig. 11-2). And

the flashing dust is not made of diamonds, but of ice crystals.

Just as you can see the sparkling drops that make garden-hose rainbows, if you are lucky you can see sparkling ice crystals right in front of your eyes that make up diamond dust halos. The bright spots in Fig. 11-1 are ice crystals, not stars, for it is daytime. Fig. 11-3 is a paradigm example of halos produced by diamond dust, especially in the eyebrow-shaped upper tangent arc at the top of the photo.

If you live where temperature falls far below 0°C,diamond dust may crystallize right in front of your eyes in the chilled air on clear cold mornings. If enough of the crystals spread around the sky, those situated where halos form with respect to the Sun will light up.

How do you find halos if they do not find you? In warmer regions, begin your search the next time cirrostratus clouds of an approaching



Fig. 11-2. Sundogs following their master, the Sun 20 Mar 2020, 21 minutes before sunset. A sun pillar also tops the Sun. Jan Curtis.

extratropical or even tropical cyclone begin to fade the sunlight. Halos can be seen on the hottest days, even at the equator, for the temperature 10 km above sea level is always cold enough for ice crystals. Of course, great care is needed not to blind yourself when looking for halos, coronas, or crepuscular rays near the Sun.



Fig. 11-3. Halo complex with 22° halo, upper and lower tangent arcs, a parhelic circle and parhelia, all lit by diamond dust crystals. ©Claudia Hinz

Instructions for Viewing Halos: While looking down, extend your arms and cross your hands to block the Sun. Then look around your

hands, preferably with sun glasses. The 22° halo will appear about an open hand width in all directions around the Sun.

If you are ever fortunate enough to witness a spectacular halo display you may find yourself swept away by its 1: huge extent, for halos may criss-cross the entire sky (both above and below the horizon), 2: blinding brightness, as with the spear tip shaped lower tangent arc directly below the Sun in Fig. 11-3, 3: high color purity, as in the circumzenithal arc near the top of Fig. 11-1, and 4: incredible variety, as in Fig. 11-1. You may then judge halos more fascinating than rainbows.

Halos can cover a greater extent of the sky than rainbows, and, of course, their scale is much greater than photographs (especially wide angle shots) suggest, for photos rarely convey a sense of the scale of the scenes they portray. The 22° halo (recall Fig. 10-41 and Fig. 10-42) is an impressive sight, for when its bottom touches the horizon its top extends half way to the zenith. But in Fig. 11-1 the 22° halo is only the *inner* ring. The outer ring, a combination of several arcs, has a *radius* of over 46°, so that if its base touched the ground, its top would extend just beyond the zenith.

We now proceed as in a mystery by first presenting the incredible variety of halos and only then explaining *how* each halo forms and how the incredible halo complexes form.

### 11.2 The Incredible Variety of Halo Forms

As of 2022, Jarmo Moilanen and Maria Gritsevich identified and listed 119 different ice crystal halos. Fig. 11-1 offers a magnificent but partial sampling of this diversity, as does Table 11-1 and Fig. 11-4, where the simulation includes and labels 17 halo forms.

Included in this great diversity are at least nine circular halos. In addition to the common 22° halo and the rare 46° halo are the parhelic circle and the so-called odd-radius halos of 9°, 18°, 20°, 23°,

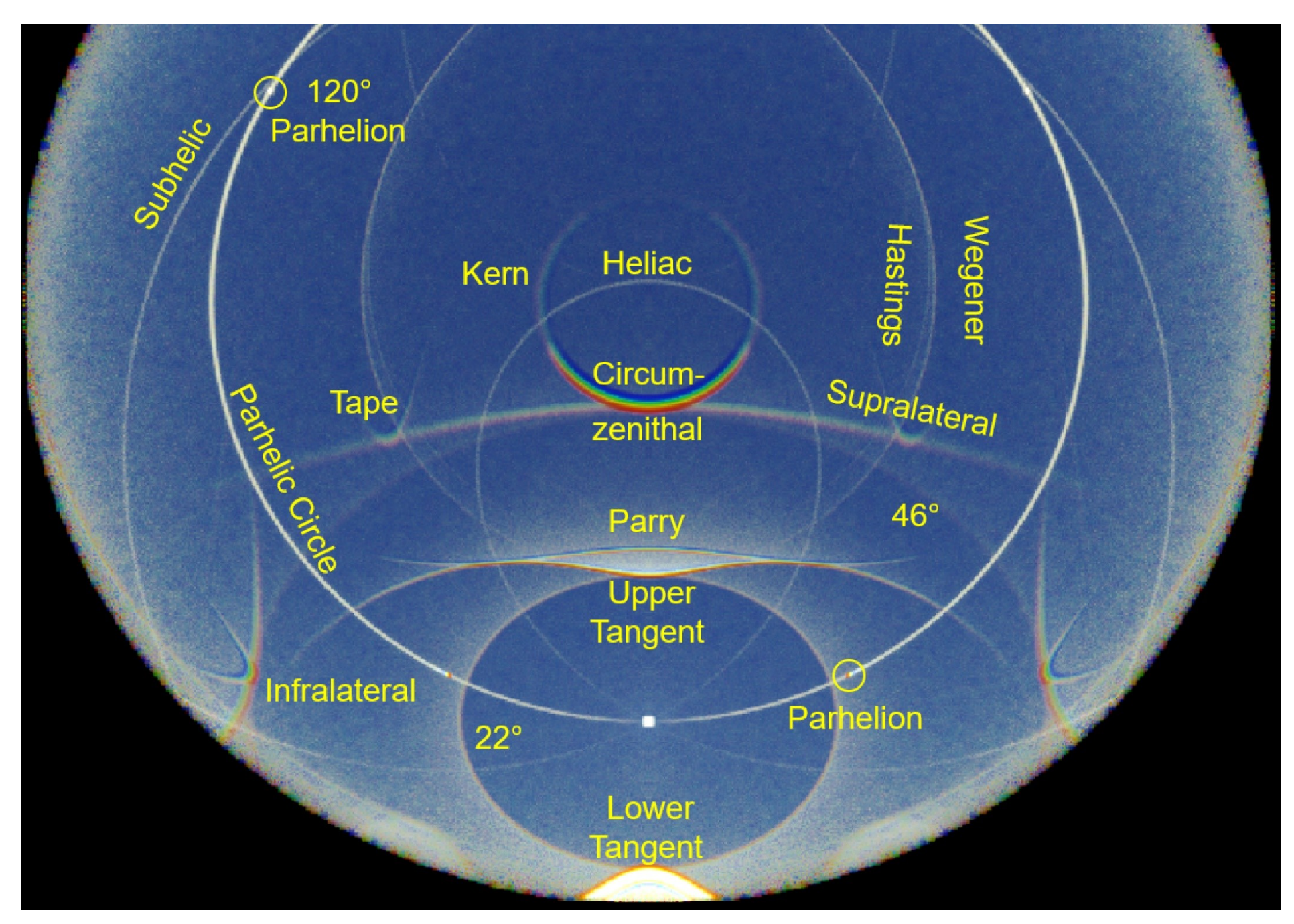


Fig. 11-4. Simulated Halo Complex for Sun height,  $H_{SUN} = 30^{\circ}$  with Halo Names. There are a few more arcs opposite the Sun (not shown here). SDG.

Table 11-1 Catalog of the more common halos and their properties.  $H_{\rm SUN}$  is the Sun's elevation angle.

Halo Name	Shape	Frequency	Intensity, Color	Crystal Shape	Orientation c-axis	$H_{ m SUN}$	Light Path
22°	Circular	High	Moderate Pale Red Inside	Plates, Pencils	Random	All	Refraction through Alternate sides
46°	Circular	Very Low	Feeble Red Inside	Thick Plates	Random	All	Refraction through 1 side and top or bottom
9, 18, 23, 35	Circular	Low	Moderate Red Inside	Pyramidal	Random	All	Refraction through at least one pyramidal face
Sundog Or Parhelion	Spot	High	Intense, Semispectral	Plates	Vertical	Below ~61°	Same as 22° halo
Tangent Arcs	Arcs at top and bottom of 22°	Medium- High	Intense, Semispectral	Pencils	Horizontal	$Below \sim 40^o$	Same as 22º halo
Circumscribed Halo	Oval around 22° halo	Medium- High	Intense, Semispectral	Pencils	Horizontal	Above $\sim 40^{\circ}$	Same as 22° halo
Parry Arcs	Arcs above and below 22° halo	Low	Intense near spectral	Pencils	A rectangular face Horizontal	All	Same as 22° halo
Circumzenithal Arc	Arc above Sun around part of Zenith	Medium- high	Bright, Spectral	Plates	Vertical	Below ~32°	Refraction in top hexagon out of side
Circumhorizon- tal Arc	Arc below Sun around part of horizon	Low	Bright, Spectral	Plates	Vertical	Above ~58°	Refraction in side out bottom hexagon
Parhelic Circle	Horizontal arc through Sun	Medium	Bright, White	Thick Plates Pencils	Vertical or Horizontal	All	Reflection from sides or Hexagons
Sun Pillar	Vertical arc through Sun	Medium-low	Bright, Same as Sun	Pencils, Plates Dendrites	Tilted slightly	Near Horizon	Reflection from top or bottom
Suprlateral Arc	Arc above Sun touching CZ arc	Low	Bright, Spectral	Pencils	Horizontal	Below ~32°	Refraction in Hexagon out of lower side



Fig. 11-5. Odd-radius halos of 9°, 18°, 20°, and 24° (with its upper tangent arc) over San Francisco, 1400 PST, 23 Feb 2016. The 35° halo was present but did not show in the photograph. ©Mila Zinkova



Fig. 11-6. Vertically elongated (overexposed) subsun surrounded by Bottlinger's Rings over the Rocky Mountains. SDG.



Fig. 11-7. Halo underworld: Subsun, sun pillar, 22° halo and lower tangent arc (on left) with subparhelion, subparhelic circle, and sub-22° halo (on right) on 11 Jan 2007, S. Canada. ©Bill Burton, USGS.



Fig. 11-8. Left: Orange Subsun and Sun pillar from a low Sun. Right: 22° halo, sundog, subsun, and lower tangent arc for  $H_{\rm SUN}$  19°. SDG.

24°, and 35° (Fig. 11-5) Most of the circular halos are accompanied by halo spots and multiple arcs. For example, the upper and lower tangent arcs are often attached to the top and bottom respectively of the 22° halo and Parry arcs sometimes bracket them. In Fig. 11-1, Fig. 11-3, and Fig. 11-4, the upper tangent arc resembles a pair of arched wings, while the upper suncave Parry arc, (concave with respect to the Sun but not visible in Fig. 11-3) appears as an eyebrow over the upper tangent arc.

There is also a whole underworld of halos. In fact, the halo with the greatest, potentially blinding brightness is the subsun, as in Fig.5-2, Fig. 10-33, and Fig. 11-6, where a faint elliptical Bottlinger ring surrounds the subsun. The subsun has its own set of halos, including a sub-22° halo and sub-sundogs, as in Fig. 11-7, which includes a sun pillar, the bottom of the 22° halo and a blinding, lower tangent arc. The detailed form of a less brilliant lower tangent arc, with a subsun near its bottom, 22° halo, parhelion, amd faint subparhelion can be seen in the right panel of Fig. 11-8.

All halo arcs change shape as the Sun's elevation angle or height in the sky,  $H_{SUN}$ , changes. Only the circular halos involving refraction appear with the same form and size at any  $H_{SUN}$ . The parhelic circle shrinks as the Sun rises and has an angular radius equal to the Sun's zenith angle,  $Z_{SUN} = 90^{\circ}$ -  $H_{SUN}$ .

As the Sun rises higher in the sky, the tangent arcs morph into the circumscribed halo as shown in the simulations of Fig. 11-9. When

the Sun is low in the sky, the upper tangent arc, which touches the top of the 22° halo, resembles a pair of arched wings, and the lower tangent arc, which touches the bottom of the halo, resembles closed legs or a spear tip, as in Fig. 11-1 and Fig. 11-3. As the Sun climbs the wings relax downward and the legs spread out and up. Once the Sun is a little higher than 30°, the upper and lower tangent arcs join to enfold the 22° halo as a circumscribed halo, as in Fig. 11-10.



Fig. 11-10. Halo display with the 22° halo surrounded by the circumscribed halo, the parhelia and parhelic circle and the rare infralateral arcs in Finland 24 Jun 2014 Sun Elevation 45°. ©Vesa Vauhkonen

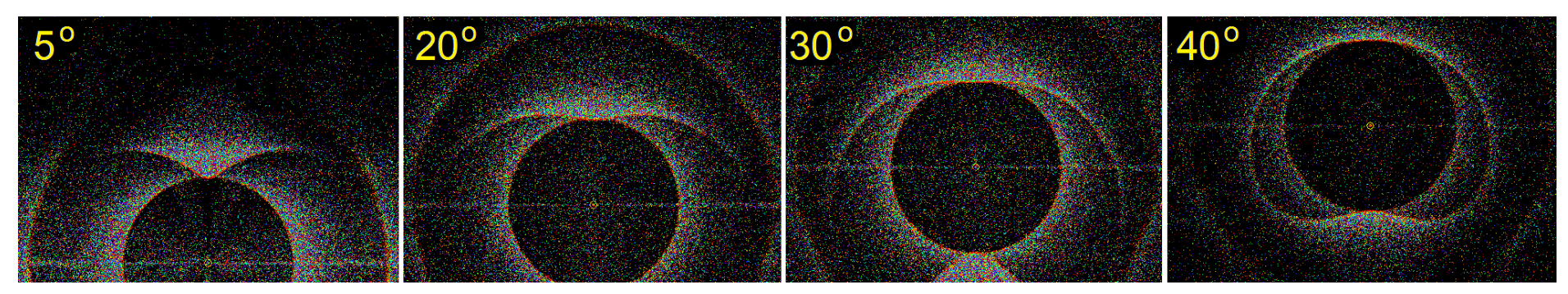


Fig. 11-9. Simulations of the 22° halo, its tangent arcs or circumscribed halo, and supralateral and infralateral arcs as functions of H<sub>SUN</sub>. SDG.

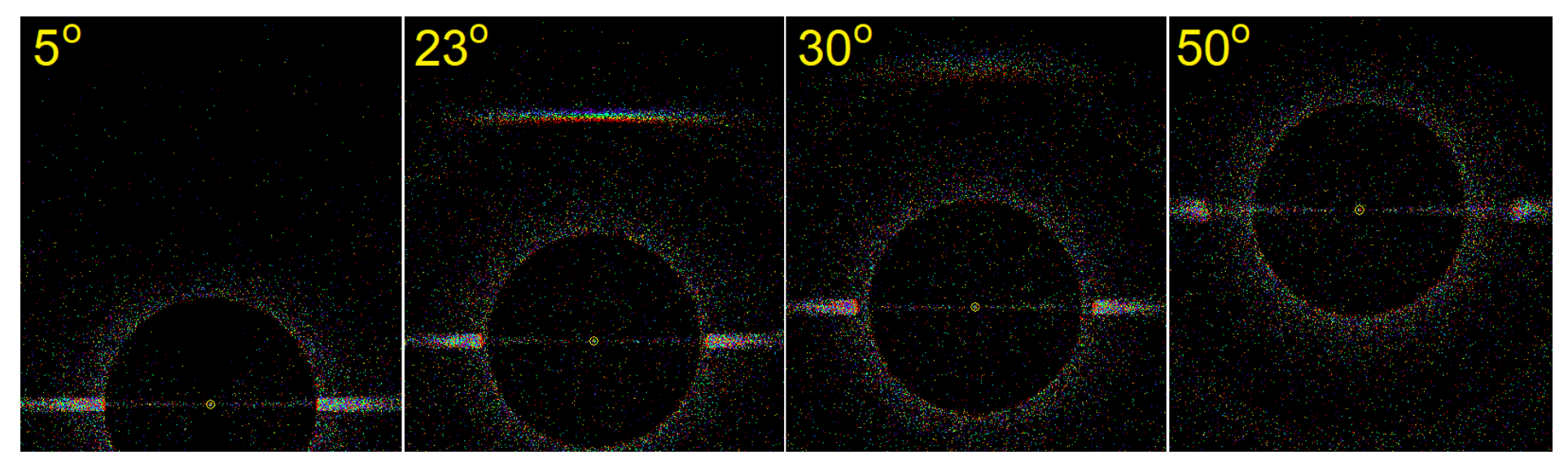


Fig. 11-11. Simulations of the 22° halo, the parhelia and parhelic circle, and the circumzenithal arc as functions of H<sub>SUN</sub>. SDG.



Fig. 11-12. Parhelic circle with 120° parhelion over Old Bald Rock Mountain, Sapphire, NC, 18 Oct 2018. SDG.

The parhelia are primarily low-Sun phenomena though they do appear for a large range of Sun heights. They form on both sides of the Sun at the same height as the Sun, which is why they are called sun dogs (following their master). When the Sun is at the horizon, the

parhelia coincide with the 22° halo. However, as  $H_{SUN}$  increases the parhelia move further outside the 22° halo, as is shown in the simulations of Fig. 11-12. In Fig. 11-9, where  $H_{SUN} \approx 45^{\circ}$  the parhelia are far outside the 22° halo and coincide with the circumscribed halo. The parhelia also tend to diminish in intensity the higher the Sun in the sky. Once  $H_{SUN} >\approx 61^{\circ}$  in the sky the sun dogs refuse to follow their master and vanish, though the parhelic circle (e. g., Fig. 11-1, Fig. 11-4, Fig. 11-9) persists and potentially brightens.

Fig 11-12 shows a piece of the parhelic circle in cirrus clouds on the opposite side of the sky from the Sun above Old Bald Rock Mountain and Fairfield Lake, NC on 18 Oct 2018 when  $H_{\rm SUN} \approx 45^{\circ}$ . The bright enlarged dot to the right of center in the parhelic circle is a 120° parhelion, which is always located at an azimuth angle of 120° from the Sun. Notice that both the parhelic circle and the 120° parhelion are white.

The parhelic circle and the 120° parhelia are among the halos that have no play of colors because they involve reflection with no refraction. Others include subsuns, the parhelic circle, the rare heliac, subhelic, Wegener, and Hastings arcs, and Sun pillars.. Since they

reflect sunlight they are near white when the Sun is much above the horizon (at least 10°) and redden as the Sun nears the horizon, as in the Sun pillars of Fig. 11-13.

It is nice to wake up seeing a sun pillar holding up the sky. Sun pillars are most pronounced around dawn, often appearing before



Fig. 11-13 Sun pillars hold the sky. 05 Apr 2025 (left). 28 Mar 2016 south of Santa Fe (center). Predawn on 10 Jan 2018 (right). Jan Curtis.

sunrise and lasting until the Sun is about  $5^{\circ}$  above the horizon. They often form in conjunction with altocumulus clouds at  $T \approx -15^{\circ}$ C, which consist primarily of supercooled droplets but obviously must contain straggler ice crystals.

More evidence that the cirrus centers of hole punch clouds consist of ice crystals is provided by the parhelion and small piece of the parhelic circle in Fig. 11-14. Coronas and iridescence but no halos, may occur in the surrounding altocumulus cloud of supercooled droplets, though they seldom do It is fun when hole punch clouds appear in the sky to seek out those that are properly located to host halos, or wait for a cirrus-filled hole to move to a possible halo location. The reward, of course, is when the cirrus lights up.

Brightness and color are two separate properties of halos, although halos that possess color tend to be brighter when they are more colorful.

Table 11-2 lists the maximum potential brightness of several halo forms relative to that of the Rayleigh atmosphere. The parhelia are the brightest of all halos seen *above* the horizon, just as subsuns are the brightest of the infernal halos. The spots are the brightest because the scattered light is directed to the smallest area of the sky. Next come the arcs, and last, the circular halos, which spread the light over the

Name	Max
Parhelion	1415
120° Parhelion	1000
Tangent Arc	92
Parry Arc	80
Parhelic Circle	34
Circumzenithal Arc	25
Heliac Arc	15
9° Halo	15
Circumhorizontal Arc	9.5
22° Halo	9.5
Parry Infralateral Arc	7.5
Parry Supralateral Arc	3.5
Hastings Arc	2.6
Subhelic Arc	2.5
Infralateral Arc	2.25
Supralateral Arc	1.65
46° Halo	1.5
Clear Skylight	1.0

Table. 11-2. Maximum potential brightness of simulated halos relative to a Rayleigh atmosphere.



Fig. 11-14. Parhelion inside hole punch cloud over Boynton Beach, Fl, 02 Jan 2024. SDG.

largest area of the sky. Some rare halo forms have great potential brightness but require stringent conditions that are seldom met.



Fig. 11-15. Circumscribed halo, parhelic circle and circumhorizontal arc over Peru with  $H_{SUN} \approx 72^{\circ}$ . ©Steve Gettle.

Color is, of course, one of the alluring properties of halos, with some halos much more colorful than others. Color even provides a way to

distinguish halos. For example, even though the colored circular halo in Fig. 11-13 seems to be a 22° halo, it is, in fact, a circumscribed halo, which is near circular at  $H_{\text{SUN}} \approx 72^{\circ}$ , and much brighter and more colorful than the 22° halo, though it is lacking in blue.



Fig. 11-16. Colorful parhelion over Boynton Beach, FL 06 Jan 2023. SDG.

The parhelia, which can be blindingly bright, never have high spectral purity. Red, which is the most prominent color of the parhelia only has modest spectral purity. Orange and yellow are progressively less pure and the 'cooler' colors are seldom seen. The parhelion in Fig. 11-16 is the most colorful that Stan remembers seeing. However, it owes its pale green and blue tones in part to the blue skylight that penetrated the optically thin cloud edge.

The most colorful halos are the arcs associated with the 46° halo, which can be seen by comparing the arcs of the 46° halo to the arcs and spots of the 22° halo in Fig. 11-1, Fig. 11-4, and Fig. 11-17, a display with the 22° halo, tangent arc, parhelia and parhelic circle, supralateral and faint infralateral arc plus the spectral circumzenithal arc. Note also that the circumhorizontal arc in Fig. 11-15 is more nearly spectral than but not as bright as the circumscribed halo.





Fig. 11-18. Circumzenithal arc over Tolland, CT 05 Dec 2010. SDG.

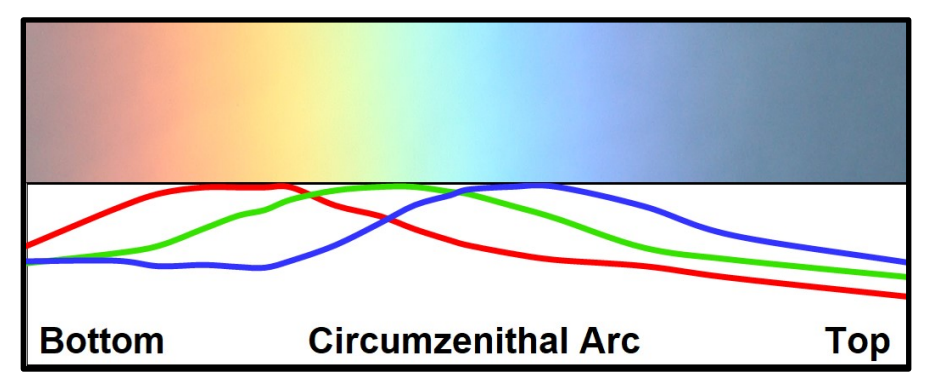


Fig. 11-19. RGB colorimetric values of vertical slice through CZ arc of Fig. 11-16. SDG.

The two most highly spectral halo arcs are the circumzenithal (CZ) arc (Fig. 11-18 with RGB values in Fig. 11-19) and the circumhorizontal (CH) arc (Fig. 11-20 with RGB values in Fig. 11-21). Not only do they have very similar spectra, they are complements of each other. The CZ arc partly circles the *zenith* at least  $46^{\circ}$  above the Sun, but only forms when  $H_{\text{SUN}} < \approx 32^{\circ}$  and its spectral purity is greatest when  $H_{\text{SUN}} \approx 22^{\circ}$ . The CH arc partly circles the *horizon* line at least  $46^{\circ}$  below the Sun, and only forms when the Sun' zenith angle,  $Z_{\text{SUN}} = 90^{\circ}$  -  $H_{\text{SUN}} < 32^{\circ}$  and its spectral purity is greatest when  $Z_{\text{SUN}} \approx 22^{\circ}$ .

The CH arc is much rarer than the CZ arc for several reasons. 1: In Polar latitudes the Sun never comes within 32° of the zenith. 2: In the mid latitudes it can only be seen in the hours around noon for a few



Fig. 11-20. Circumhorizontal arc over Nepalese Himalayas, 7 May 2011. Фтещт Нфтлщмнш.

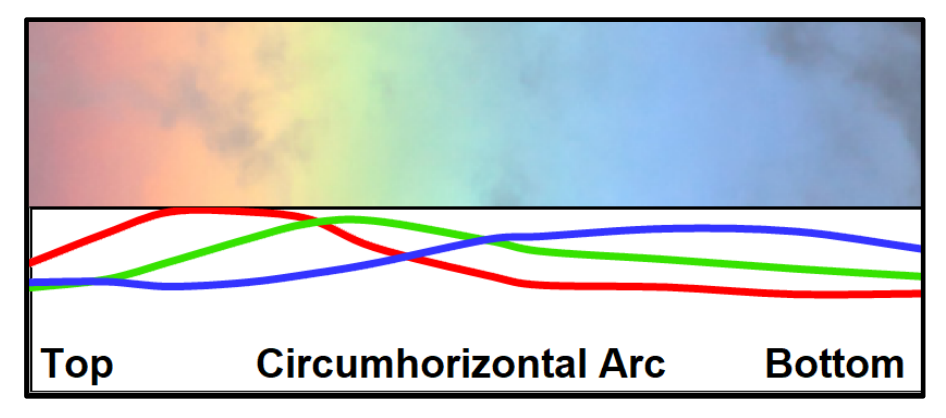


Fig. 11-21. RGB colorimetric values of vertical slice through CH arc of Fig. 11-18. SDG.

weeks or months around the summer solstice in mid-latitudes, a time when most cirrus are tainted by 'junk' (non-crystalline) ice. 3: Near the equator it can potentially be seen any day of the year near the equator in the hours near noon, where anvils with 'junk' ice dominate. By contrast, the CZ arc can be seen any day with sunlight.

## 11.3 Why Halos are so Varied

We have now seen a significant number of different halos, though only a few of the 119 halos are common. The most common seen from the ground are the 22° halo and the parhelia, which are observed almost 200 days a year in Western Europe! Many halos are

quite uncommon and some, such as the Kern and Lowitz Arcs, and sun dog of the sun dog are so rare they may not be reported anywhere in a generation. Nevertheless, all these halos do exist. How can there be so many when there are only four rainbows (aside from virtually invisible higher order bows)?

Begin with the analogy between ice crystals and cut diamonds. Turn a brilliant cut diamond ever so slightly and whole series of sparkles flash on and off. The popular *brilliant cut* for diamonds was designed in 1919 by Marcel Tolkowsky using a combination of trial and error and mathematics to maximize sparkle. The sparkles are due to the fact that the brilliant cut diamond has 57 facets with the optimal dimensions and angles. The most basic ice crystal plan is the hexagonal prism with only 8 facets (six rectangular side faces and two hexagonal end faces), but that's enough for starters. Pyramidal crystals have up to 12 additional facets By contrast, raindrops and cloud droplets are not faceted.

The great diversity of halos arises from the large number of choices a sunbeam has. It can strike any of the facets (showing its face to the Sun) and either be reflected by or refracted into the crystal. Once inside the crystal it can be refracted immediately upon striking another facet or reflected once or more inside the crystal before ultimately being refracted and leaving the crystal.

The choices available to the sunbeams and the angles of deflection derive from three geometrical factors,

- 1: The shape of the ice crystals,
- 2: Their orientation as they fall,
- 3: The Sun's height in the sky.

These factors, along with the laws of reflection and refraction and Fresnel's Law determine which facet the sunlight strikes, which facet it leaves, the angle, D, it has been deviated by, and the fraction of light beams reflected or refracted at each facet.

The brightness of halos depends on two additional factors,

- 4. The size of the ice crystals,
- 5. The optical thickness of the cloud and atmosphere.

As with raindrops, geometric optics is an excellent approximaton for how ice crystals larger than about 100 µm scatter light. Diffraction, which only vitiates halos, (there are no supernumerary halos) becomes increasingly important the smaller the crystals.

The optical thickness through the cloud determines the probability that light will emerge from the cloud after striking one and only one crystal. The optical thickness through the atmosphere, including the effect of aerosols, diminishes the halo beam and determines the contrast-reducing background lighting.

### 11.4 Forms of Ice Crystals

The study of halos represents a marriage with the study of ice crystals. Almost always, the simplest ice crystals make the best halos. The most basic ice crystal form is the 8-facet hexagonal prism.

It has 6 rectangular sides (prism faces) of length, c and 2 hexagonal ends (basal faces) of width, a. The ratio (c/a) of crystal length to width, is the aspect ratio. The direction of the crystal is defined by the c-axis, which points out from a hexagonal face, and by the angle the rectangular faces rotate around the c-axis

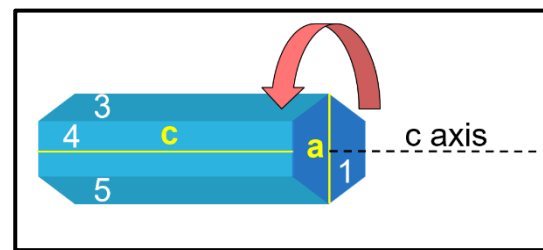


Fig. 11-22. A simple pencil ice crystal of length c > width a, with faces numbered. Pencil crystals often fall with c-axis horizontal and may spin around the c axis. SDG.

Pencil crystals are much longer than wide and have typical aspect ratios of about 3 to 5. Plate crystals are much shorter than wide and have typical aspect ratios of about 0.2 to 0.33. Pencil crystals often fall with c-axis horizontal (as in Fig. 11-22) while plate crystals tend to form with the c-axis vertical.



Fig. 11-23. Ice crystal forms. ©Kenneth Libbrecht

Crystals may grow pyramidal endings, either on one or both basal faces. The pyramids are either complete, coming to a point, or stunted and ending at a smaller basal face, in which case a bipyramidal crystal will have 20 facets. The length of a complete pyramid is always 1.63 times its width (aspect ratio = 1.63). The angle between the c-axis running the length of the prism and each of the pyramidal sides is  $28^{\circ}$ . Walt Tape (a leader in collecting diamond dust crystals that produced halo complexes at the South Pole) has dubbed this *Angle x* because it took two centuries to determine.

Simple, solid pencil, plate, and pyramidal ice crystals are the exception. The vast majority of crystals have complex features, including capped ends, hollow insides, steps, and spiked branches (Fig. 11-23). Each of these complexities reduces the halo producing effectiveness of the crystals. Star-shaped crystals (*dendrites*), as beautiful and symmetric as they are, are so complex, with so many facets, that the only halos they can produce are subsuns and sun pillars. It should be obvious that heavily rimed and multifaceted

crystal complexes, such as in Fig. 11-24, cannot produce any halos at all. For the purpose of halos, they are 'junk' ice.

It took time to sort out the crystal forms and their properties. The microscopic study of ice crystals was pioneered by Robert Hooke (*Micrographia*, 1665). Explorer, and natural scientist William Scoresby furthered the field in

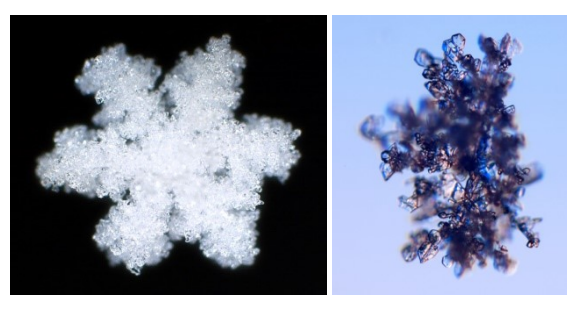


Fig. 11-24. Heavily rimed snowflake and a crystal cluster. ©Kenneth Libbrecht.

around 1820 with his drawings of pristine crystals observed in the Arctic, documenting the basic forms, including plates, pencils, and pyramids or bullets in addition to the well-known star-shaped crystals.

Starting in the late 1800's and continuing up to his death in 1931 from pneumonia contacted in a snowstorm, Wilson Bentley in Vermont pioneered the microscopic study of snow crystals, photographing them resting on black velvet with great skill and selection. (He apparently rejected thousands of flakes for each one he chose.) Taking up where (and when) Bentley left off, Ukichiro Nakaya in Japan documented the ranges of T and RH under which the various forms of ice crystals dominate and illustrated them in a Nakaya Diagram (Fig. 11-25).

For example, plates dominate for the ranges,  $0^{\circ}\text{C} < \text{T} < -3^{\circ}\text{C}$  and  $-10 < T < 20^{\circ}\text{C}$ , while columns dominate in the range,  $-3^{\circ}\text{C} < T < -10^{\circ}\text{C}$  Solid plates dominate at the smallest values of supersaturation over a large range of temperature. In general, crystal complexity increases with the degree of supersaturation, with star-shaped or dendritic crystals dominating at the highest values of supersaturation, especially in the range,  $-10 < T < 20^{\circ}\text{C}$ .

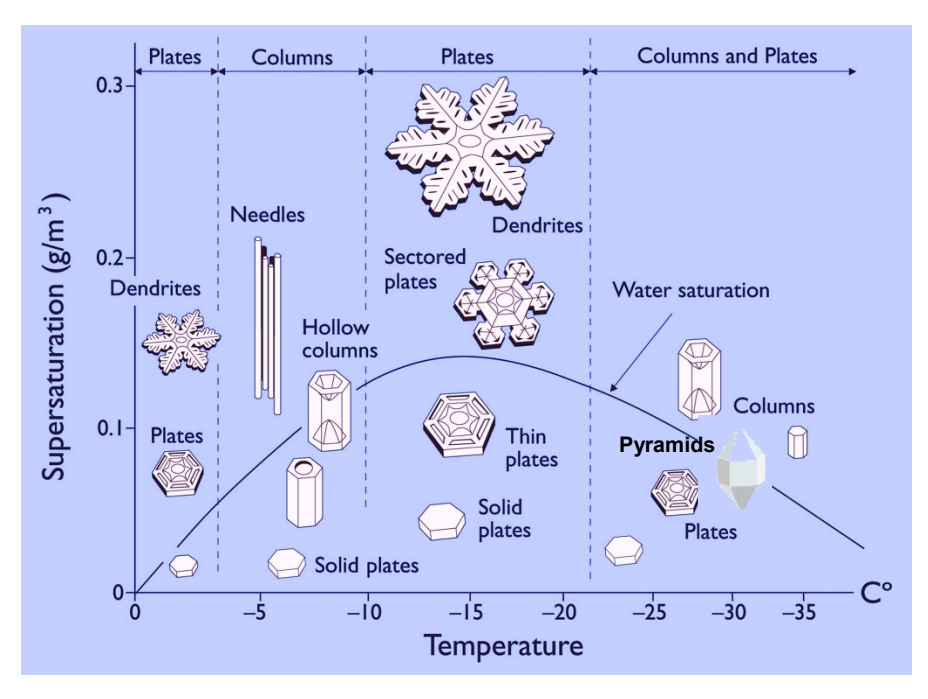


Fig. 11-25. Nakaya Diagram of ice crystal growth habit vs T and RH. ©Kenneth Libbrecht.

Kenneth Libbrecht has advanced this work by elucidating the growth mechanisms of the crystals. In order for vapor molecules to deposit on ice crystals they must overcome an energy barrier. Hexagonal faces have a different energy barrier than rectangular faces. In the temperature ranges where plates dominate, the energy barrier is smaller at the edges of the hexagonal faces, so depositing vapor molecules extend the hexagonal faces. When supersaturation is low, growth is slow and vapor molecules tend to fill in gaps in crystals, leading to solid forms. When supersaturation is high, growth is rapid and vapor molecules from the ambient atmosphere find the places where the crystal protrudes into the environment the most, hence the crystal grows branches and spikes on the branches to form stars.

The amazing symmetry amidst the profound complexity of the starshaped crystals, with all branches almost identical, leads to a natural but bogus question, "How does each branch 'know' what the others are doing?" The fact is, the branches don't 'know' anything. What happens is that as the crystal passes through the cloud each branch is bathed in almost identical variations of temperature and saturation ratio, so that the growth of each branch is near identical.

In recent decades, ice particle censuses in clouds have been taken by laser cloud particle imagers on instrumented aircraft. Thunderstorm anvils contain mostly 'junk' ice thrust upward from lower in the cloud, often as droplets that froze upon contact with ice particles (rime). Even in the stratiform cirrostratus clouds of extratropical cyclones there are enough embedded convective cells to loft a substantial fraction (at least 33%) of rimed ice particles.

What this means for halo lovers is depressing. It renders the bulk of ice clouds at best poor halo producers, and the good halo producers as exceptional. This is one main reason why many of the best halo producers are the thin and often almost invisible ice fogs that slowly grow the diamond dust on frigid days in the polar regions and on frigid winter mornings in the higher middle latitudes.

## 11.5 Crystal Orientation and Halo Forms

Orientation of crystals as they fall is the second factor that determines halo form. The simplest, and potentially brightest of all halo forms, especially when the Sun is low in the sky, is the *subsun* (Fig.5-1, Fig. 10-32, and Fig. 11-6). It is a spot produced by sunlight reflected from plate crystals (or dendrites) that fall with horizontal hexagonal basal faces (vertical c-axis). The subsun appears directly below the Sun, and as far below the horizon as the Sun is above it.

Sunbeams reflected from the vertical rectangular side faces of plate crystals produce the *parhelic circle*. It appears at the same elevation angle as the Sun,  $H_{SUN}$ , but at varying angles off to the side depending on the crystal's rotation around the c-axis.

The orientation of falling crystals is a result of aerodynamic forces. Large objects tend to tumble turbulently in all directions as they fall. Small objects, such as ice crystals tend to fall smoothly, with the largest area near horizontal, which ironically maximizes drag. In the

land of maple trees, it is a common wonder to see the autogyrating winged seeds or *samaras*, heavy on the end with the encapsulated seed, fall like whirling helicopter wings, their flat blades almost horizontal. A simple experiment is to cut rectangular and triangular pieces of paper, about 5 cm long and 1 - 2 cm wide and watch as they fall. Within a meter of their release they settle into a stable fall pattern, spinning rapidly about their long axis, which remains almost horizontal, while their path traces out a helix.

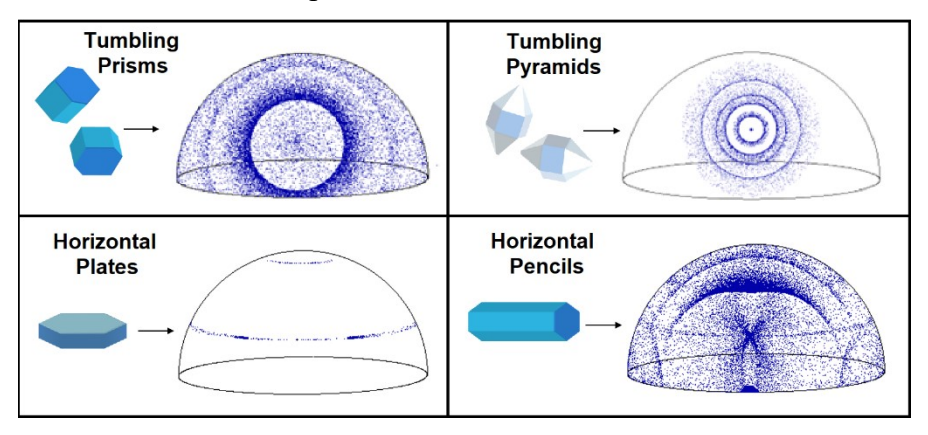


Fig. 11-26. Halo Forms vs Ice Crystal Habit and Orientation. SDG.

The main simple, ideal crystal forms, their common orientations as they fall, and the halos they produce are shown in Fig. 11-26. Thick crystals, with aspect ratios near 1, tend to tumble in all directions as they fall, scattering the light in all directions around the Sun. Therefore, randomly oriented crystals produce the circular halos. The simple, 8-faceted crystals, produce the 22° and 46° halos while the crystals with pyramidal faces produce the uncommon odd-radius 9°, 18°, 20°, 23°, 24°, and 35° halos.

Flat, plate-shaped crystals tend to fall with the wide hexagonal basal faces horizontal (the c-axis vertical). They produce the parhelia and the parhelic circle, and, depending on  $H_{SUN}$ , the CZ or CH arcs and their infernal versions as well.

Long pencil-shaped crystals tend to fall with the long, c-axis horizontal. They produce the tangent arcs to the 22° halo or the

circumscribed halo when the Sun is higher than  $\sim 40^{\circ}$ , and the supralateral and infralateral arcs, among others, depending on  $H_{SUN}$ .

Some of the rare arcs only form with extra restrictions on the fall modes of the crystals. The Parry arcs require not only that the c-axis of pencil crystals be horizontal, but that two opposite rectangular prism faces be near horizontal as well. Although there is no established aerodynamic reason why crystals should fall with a rectangular face horizontal, geometric optics calculations and computer simulations of halos have certified this double restriction on crystal orientation does in fact exist. Hypotheses include 1: pencil crystals with basal faces of unequal sided (scalene) hexagons, and, 2: Parry oriented pencils locked in a crystal cluster.

## 11.6 Geometric Optics of Halos

Explaining and modeling halos with geometric optics use the same laws used with rainbows – the law of reflection, the law of refraction, and Fresnel's Law. The huge difference is that rainbows are modeled using spherical (or near spherical) drops, which renders the problem almost two dimensional and the geometry simple. Halos are modeled with crystals of different forms, orientations, and complex relations to  $H_{\text{SUN}}$ . These differences make the halo problem far more intricate if not more difficult.

So, let's start with the simplest scenarios.

### 1: Beam Paths for the Halos and their Arcs and Spots

The 22° halo and its arcs and spots are produced by light beams that refract on entering a rectangular face and refract a second time on exiting an *alternate* rectangular prism face (Fig. 11-27 left panel). Light beams that strike the *opposite* rectangular face and exit the crystal leave at the same angle they entered with no net refraction and no dispersion. Beams strike *adjacent* sides too obliquely to exit the crystal, i. e., at an angle larger than the critical refraction angle

(recall Chapter 1) for ice of  $r_{\rm crit} \approx 49^{\rm o}$ . Such beams are totally internally reflected and will exit some other face.

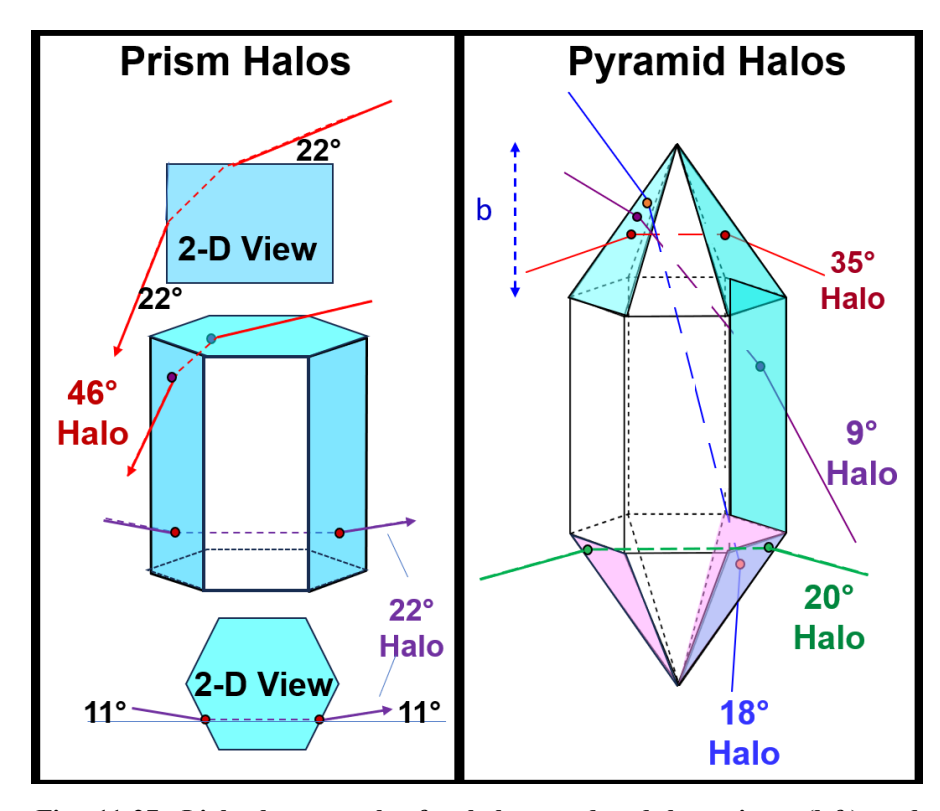


Fig. 11-27. Light beam paths for halos produced by prisms (left) and pyramids (right). For circular halos c-axis takes all values, not just vertical. SDG.

The 46° Halo and its arcs are produced by beams that refract as they pass through a hexagonal basal face and a rectangular side.

The odd-radius halos and their arcs are produced by pyramidal crystals. The right panel of Fig. 11-27 shows the paths for 4 of the 6 odd-radius halos. Beams for the 9° halo pass through a pyramidal face and the opposite rectangular prism face. Beams for the 18° halo pass through alternate pyramidal faces on opposite pyramids. Beams for the 20° halo pass through opposite pyramidal faces of the same pyramid. Beams for the 35° halo pass through alternate pyramidal faces of the same pyramidal face and the opposite prism face. Beams for the 23° halo

form in truncated pyramidal crystals and pass through one pyramidal face and one hexagonal basal face.

Beam paths that produce halos, arcs, and spots for plate and pencil prism crystals of various orientations are given in Fig. 11-28.

#### 2: Minimum Deviation Angle, $D_{min} \rightarrow Maximum Brightness$

The  $22^{\circ}$  halos of 24 Jan 2022 over Cheyenne (Fig. 10-44) produced in cirrostratus with -55 < T < -35 and on 08 Jan 24 at the Pizon ski slope in Switzerland in ice fog (Fig 11-29) are exemplary cases even

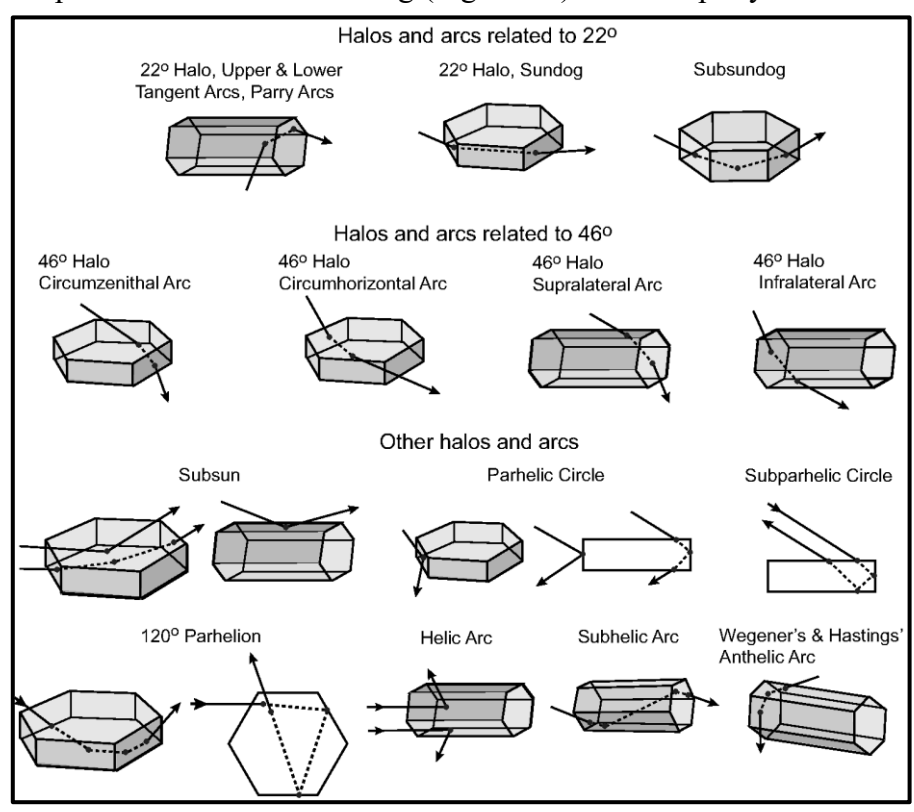


Fig. 11-28. A halo itinerary with the shapes and orientation of crystals, and the paths of light. @Kuo-Nan Liou

though they are neither blinding nor colorful. Recall from Table 11-2 that though the 22° halo is the most common halo form, its maximum brightness is tiny compared to many other halos. These halos have

the typical slightly red inside rim and one more striking feature (after it is pointed out). The sky inside the halos is darker than outside. The contrast for the 22° halo is dramatized by the Monte Carlo dot model simulations of Fig. 11-9, Fig. 11-11, and Fig. 11-30, excluding skylight. The right panel of Fig. 11-30 shows that at 22° the number concentration of dots rises abruptly from low values and then quickly decreases as the deviation angle continues increasing.



Fig. 11-29. 22° halo, parhelia and parhelic circle in ice fog Pizol Ski Area Switzerland 08 Jan 2024. ©Robert Gedzelman.

The sky is darker inside the 22° halo because 22° is the minimum angle sunbeams can be deflected by when passing through alternate rectangular side faces of ice crystals. Fig. 11-31 shows that the deviation angle,  $\bf{D}$  is a minimum.  $\bf{D}_{min} \approx 22^{\circ}$  when the angle of incidence,  $\bf{i} \approx 41^{\circ}$ . Fig. 11-32 shows that for  $\bf{D} > \bf{D}_{min}$  the relative number of beams calculated from Fig. 11-31 for each 0.1° range of  $\bf{D}$  decreases by over 80% within 1° of its maximum at  $\bf{D}_{min}$ . The 22° halo continues fading outward until it vanishes at  $\bf{D}_{max} \approx 50^{\circ}$ .

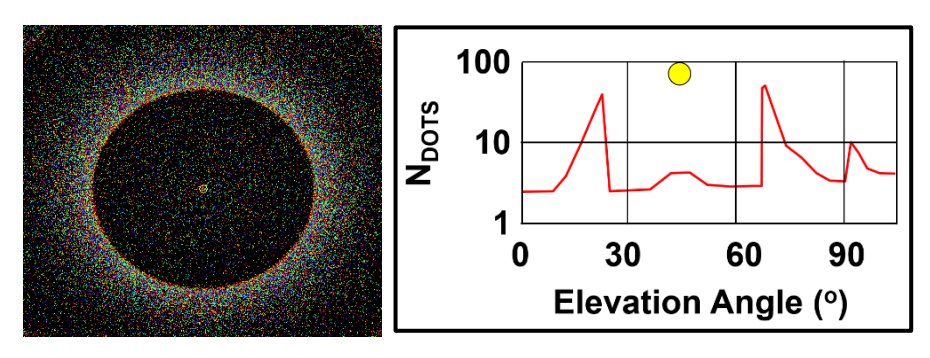
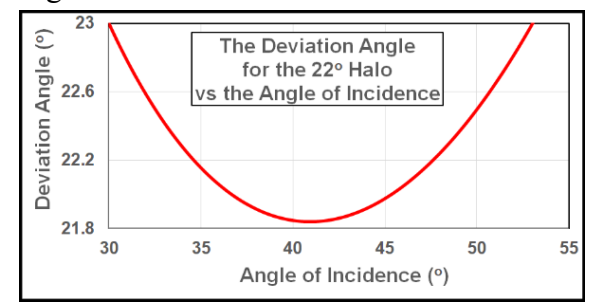


Fig. 11-30. Dot model of the 22° halo (left) and relative number of beams vs angle (right) produced by thick, random oriented plate crystals. SDG.

Color arises at the inner edge of the 22° halo because red is deviated

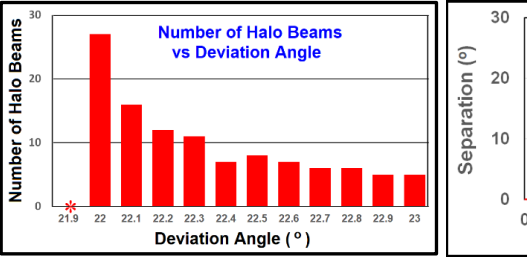
less than the other colors. Thus, the halo is not only brightest but also most colorful near its inner edge, where the overlap of colors is minimized, as with rainbows.



The calculations made for Fig. 11-31 and Fig.

Fig. 11-31. Angle of incidence on crystal i vs deviation angle,  $D_{\min}$  for the 22° Halo. SDG.

11-32 apply to crystals with c-axis is oriented at right angles to the



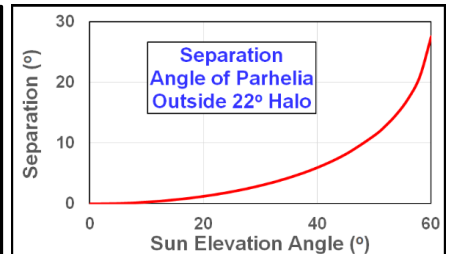


Fig. 11-32. Number of beams vs D for Fig. 11-33. Angle of parhelia outside the 22° halo. SDG. 22° halo vs  $H_{SUN}$ . SDG.

sunbeams. For randomly oriented crystals, the angle between the sunbeams and the c-axis takes all values from  $0^{\circ}$  to  $90^{\circ}$ , and the more obliquely the beams strike the crystal, the larger the value of  $\boldsymbol{D}_{\min}$ .



Fig. 11-34. A colorful parhelion outside a faint 22° halo for  $H_{\rm SUN}\approx 28^\circ$  over Cheyenne, WY, 10 Dec 2018. Jan Curtis

The parhelia illustrate how the minimum deviation angle,  $\boldsymbol{D}_{\min}$ , increases as the angle between the sunbeams and the c-axis decreases. The parhelia form when plate crystals fall with the c-axis vertical and light passes through two alternate vertical rectangular faces. The higher the Sun the more obliquely beams strike the vertical rectangular faces and thus the larger the value of  $\boldsymbol{D}_{\min}$ , and

the further outside the 22° halo the parhelia form (Fig. 11-33). This was illustrated in the simulations of Fig. 11-11 and by comparing how far the parhelia lie outside the 22° halo in Fig. 11-29, when the Sun is low in the sky, the halo with the colorful parhelion in Fig. 11-34 when  $H_{SUN} \approx 28^{\circ}$  and Fig. 11-9 where  $H_{SUN} \approx$ 



Fig. 11-35. Closeup view of the parhelion in Fig. 11-34. Jan Curtis.

45°. An enlarged view of the parhelion (Fig. 11-35) highlights its impressive range of colors including seldom seen blue in parhelia.

Parhelia are seen more often and tend to be more intense the lower the Sun in the sky (though not all the way to the horizon) for the same reason that the lower the Sun in the sky the more likely that sunlight passing into a room through a window will strike the opposite wall than the floor. The probability of striking the opposite wall also increases as the room's height to width ratio (its aspect ratio) increases. Similarly, the thicker the plate crystal in relation to its height (i. e., the larger its aspect ratio) the more likely the sunbeams will strike an alternate vertical face and not the hexagonal base.

The maximum potential number concentration of beams producing the parhelia as a function of crystal aspect ratio for  $H_{SUN}$ from 5° to 50° (calculated by a Monte Carlo halo model that neglects atmospheric obscuration) is given in Fig. 11-36. It shows that when the  $H_{SUN}$  is 10° or less, 1: the

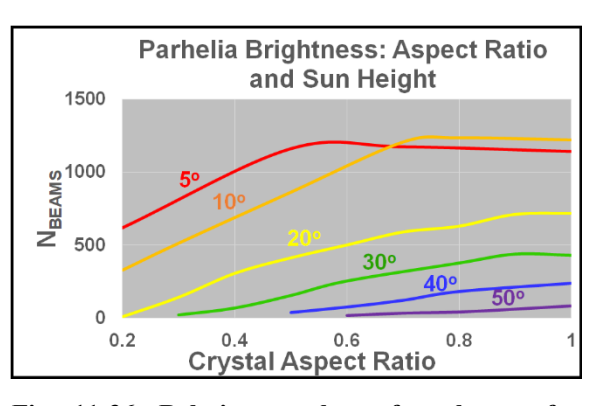


Fig. 11-36. Relative number of sunbeams for parhelia as a function of crystal aspect ratio for various values of  $H_{\text{SUN}}$ . SDG.

parhelia can be more than 10 times brighter, and 2: can occur for much thinner plate crystals, than when  $H_{SUN} > 40^{\circ}$ .

High-Sun parhelia suffer from a further major limitation. Since they can only be produced by relatively thick plates, and since the aerodynamic force that keeps thick plates falling with c-axes vertical is weak, thick plate crystals are more likely to tumble with all orientations. That would produce a 22° halo but no parhelia.

In any case, once  $H_{SUN} > \approx 61^{\circ}$  the parhelia disappear because all beams strike the alternate rectangular prism face at above the critical angle and are totally internally reflected.

The tangent arcs of the 22° halo are produced by horizontal pencil crystals that spin at all angles around the horizontal c-axis. They are tangent to the top and bottom of the 22° halo because there, the c-axis is perpendicular to sunbeams and because as the crystals spin around the c-axis all values of incidence angle, i, (including  $i \approx 41^{\circ}$ ) occur for some crystals, as in Fig. 11-31. Moving to either side of the tangent arc, the sunbeams confront the rectangular sides more

obliquely, so the tangent arcs wing their way further outside the 22° halo.

Fig. 11-9 shows that the higher the Sun in the sky the lower the 'wings' of the tangent arc until at  $H_{SUN} \approx 32^{\circ}$  the upper and lower tangent arcs join to form the circumscribed halo.

The higher the Sun in the sky, the closer the circumscribed

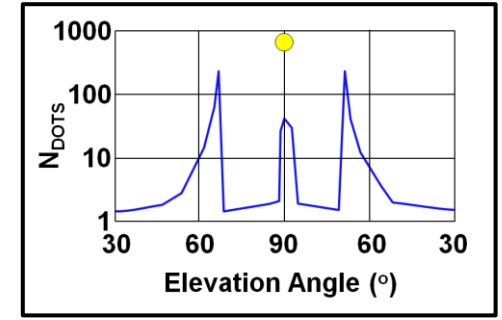


Fig. 11-37. Relative number of beams vs angle produced by pencil crystals with horizontal c-axes is 4x greater than for the 22° halo. SDG.

halo approaches the  $22^{\circ}$  halo, as in Fig. 11-13, until when the Sun is at the zenith, the two merge. But there are differences. The restriction on crystal orientation for the circumscribed halo makes it narrower, more colorful and about four times brighter than the  $22^{\circ}$  halo. (Compare  $N_{dots}$  in Fig. 11-37 with the right panel of Fig. 11-30.)

If, in addition, pencil crystals with horizontal c-axes have the further restriction that two rectangular sides are also horizontal (the orientation for Parry arcs), then the resultant circular halo when the Sun is at the zenith is 25% brighter than the circumscribed halo, has an almost spectral color sequence, but has an angular radius of 25° ( 3.1° larger than the 22° halo) because the angle between the rectangular sides the refracted beams pass through and the vertical sunbeams is 30°. In addition, the restriction imposed by the Parry orientation (with maximum 1° tilts) eliminates the spread of dots that occurs for randomly oriented crystals and crystals that can rotate around a fixed c-axis. Side-by-side comparison of Monte Carlo dot models of the 22° halo, the circumscribed halo, and the larger, brighter, spectral Parry halo in Fig. 11-38 illustrate these differences.

Parry arcs (there are several) are potentially brilliant and colorful, but

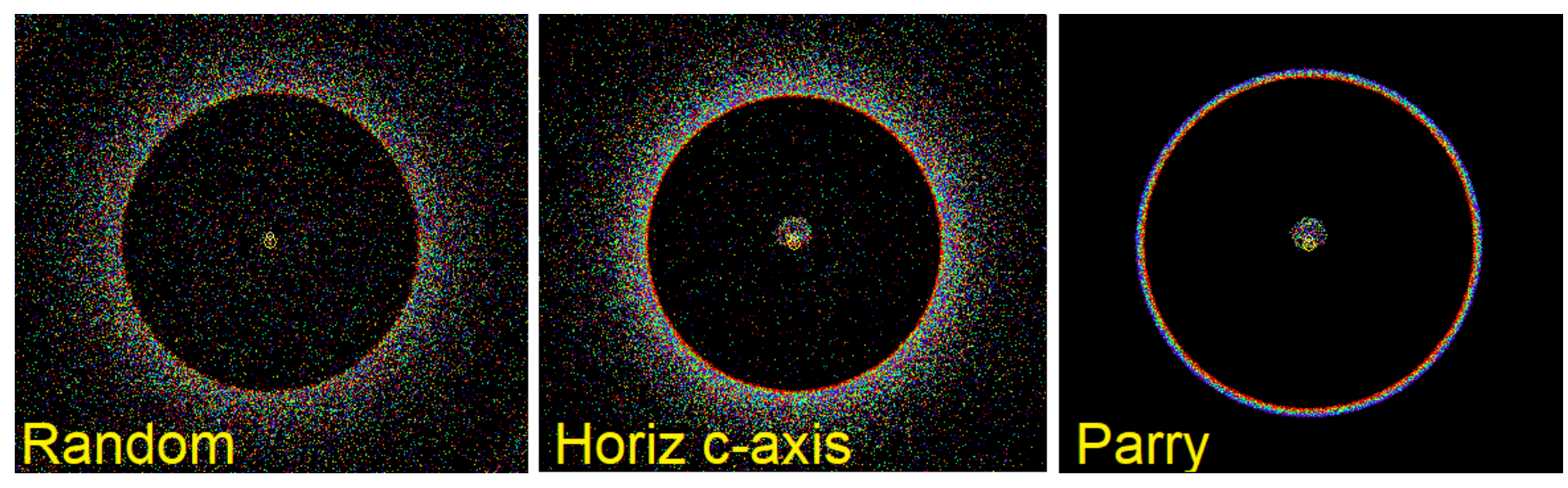


Fig. 11-38. Comparison of dot density and color purity for the 22° halo (left), circumscribed halo (center) and 25° Parry halo (right) for Sun at the zenith. SDG.

relatively rare, potentially beautiful, and curious critters because of the extra restriction that two rectangular faces be horizontal. Not surprisingly, Parry arcs are prominent in the even rarer complex halo displays such as Fig. 11-1 and several in §11.7. In these displays only the eyebrow-shaped suncave Parry arc appears.



Fig. 11-39. Halo Display over Cheyenne, WY, 23 Nov 2019 for HSUN  $\approx 6^{\circ}$  with upper tangent arc, sunvex Parry arc, circumzenithal arc, 22° halo, parhelia, parhelic circle, and a seventh arc. Jan Curtis.

The complex halo display of Fig. 11-38 contains both a faint suncave Parry arc and much brighter wing-shaped sunvex Parry arc. The wing-shaped sunvex Pary arc appears above and within the upper tangent arc that touches the 22° halo. The display also includes a parhelion and the parhelic circle, and the colorful circumzenithal arc. Why do both Parry arcs remain well outside the 22° halo and not touch it as the tangent arc does? It's all a matter of angles. Because

the crystals that form the Parry arcs do not have the freedom of rotating around the c-axis but remain locked with two opposite rectangular side faces kept horizontal, no sunbeams can strike the crystals at the optimal angle of 41° required to produce  $\boldsymbol{D}_{\text{min}} \approx 22^{\circ}$  except when  $\boldsymbol{Z}_{\text{SUN}} \approx 41^{\circ}$ .

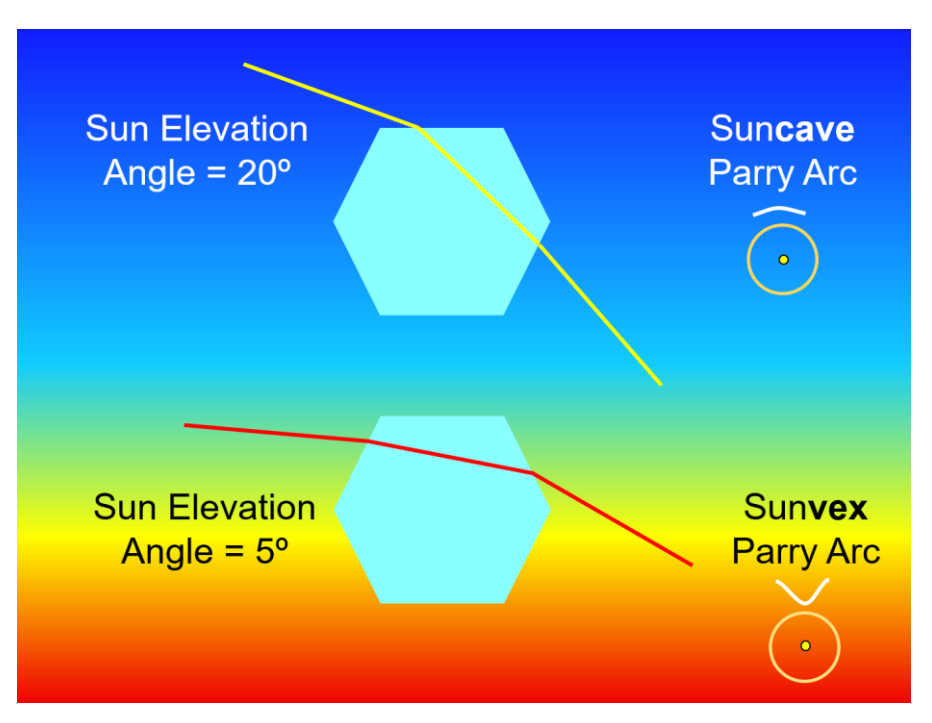


Fig. 11-40. Sunbeam paths for the upper Suncave and Sunvex Parry Arcs. SDG.

What makes the Parry arcs curious is that sunbeams have two distinct paths (Fig. 11-40), which leads to two distinct arcs. Sunbeams can either enter the top horizontal face to produce the suncave Parry arc, or an adjacent upward tilted face to produce the sunvex Parry arc. When  $H_{\rm SUN} < \approx 7^{\circ}$ , only the sunvex Parry arc appears (unless the pencil crystals have an aspect ratio of at least 5. When  $H_{\rm SUN} > \approx 17^{\circ}$  (as in Fig. 11-1), only the suncave Parry arc forms. For the intermediate range of  $H_{\rm SUN}$ , both Parry arcs are visible. These properties of Parry arcs are illustrated in the simulations of Fig. 11-41, which allow tilts of the c-axis and the rectangular side up to 1° for a range of  $H_{\rm SUN}$  for crystal aspect ratio, 3.

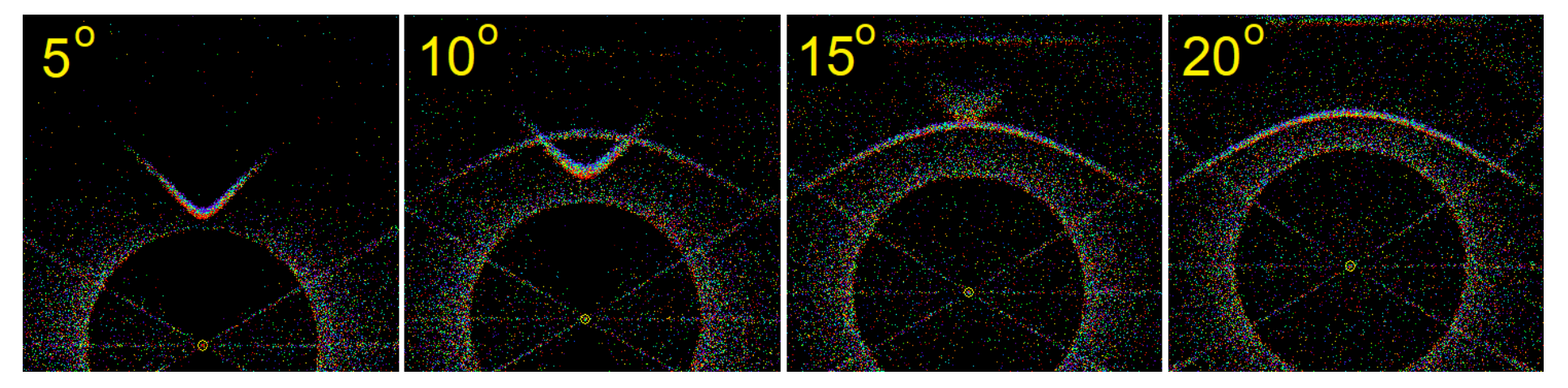


Fig. 11-41. Monte Carlo dot model simulations showing dependence of suncave and sunvex Parry arcs on HSUN, with 22° halo to provide scale. SDG.

Stan's attempt to simulate the halo display in Fig. 11-39 contituted a form of detective work common when simulating halos and halo complexes. The Sun's height is essential data. The display formed in a cirrostratus cloud at the top of the troposphere at  $T \approx -53^{\circ}$ C and was photographed 37 minutes before sunset, at which time  $H_{\text{SUN}} \approx 6^{\circ}$ .

In the attempt to reproduce the display accurately on the computer, the Monte Carlo halo dot model was run many times. The first runs, assuming Parry-oriented pencil crystals with the typical aspect ratio = 3 failed to produce the suncave Parry arc. Because the mystery arc was  $\approx 40^{\circ}$  above the Sun and hence near arcs of the 35° halo, stunted pyramidal tops were added to the thin, horizontally oriented plate crystals (c-axes vertical). That succeeded in producing a suncave arc that matched the photograph but was too bright.

This was not satisfactory, in part because of the brightness but mainly because introducing stunted pyramidal crystals was unlikely, so more computer runs were made. Lo and behold long Parry-oriented crystals with aspect ratio at least 5 did, in fact, produce a weak suncave Parry arc that closely matched the photograph. Both alternatives (long pencils vs pyramidal capped plates) are shown in Fig. 11-42. Crystal characteristics for this simulation are listed in Table 11-4, and we continue the presentation of this simulation when treating complex halo displays in §11.7.

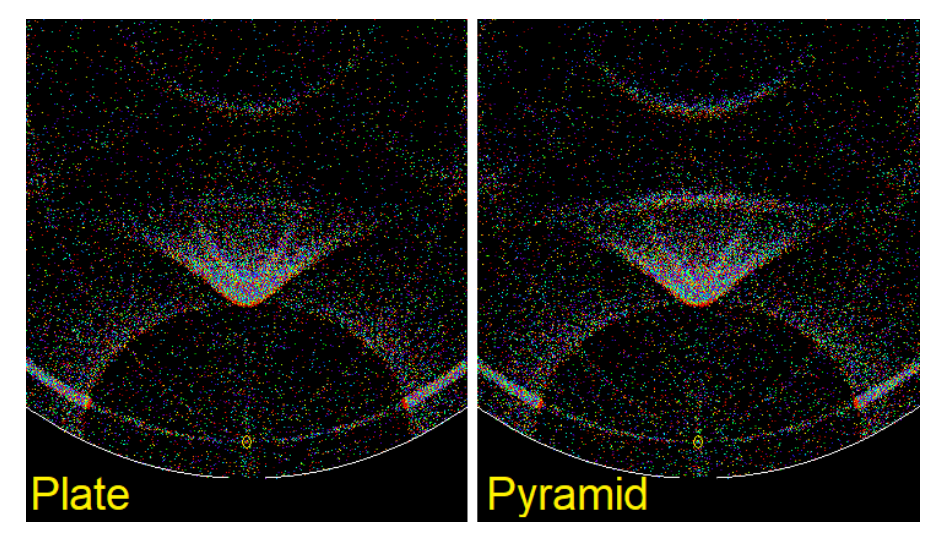


Fig. 11-42. Monte Carlo dot simulations of the halo display of Fig. 11-34 with plate crystals (left) and truncated pyramids (right). SDG.

The 46° halo and its various arcs form when sunbeams refract through one rectangular side and one hexagonal face (Fig. 11-27 and Fig. 11-28). For these arcs,  $\boldsymbol{D}_{\text{min}} \approx 46^{\circ}$  occurs only when the plane of the beams occurs at right angles to the rectangular side face they enter or exit the crystal.

The 46° halo, which forms from randomly oriented prisms, is quite rare. That is surprising considering that simulations with randomly oriented crystals show it present whenever the 22° halo appears, albeit much fainter. But it is not surprising, considering that many crystals have hollow or stepped ends (as in Fig. 11-23) and not flat hexagons.

The most common of the 46° halo arcs is the circumzenithal CZ) arc. Halo displays including the CZ arc often include the parhelia, implying that they are usually produced by plate crystals falling with the c-axis vertical, though they can be produced by Parry oriented crystals.

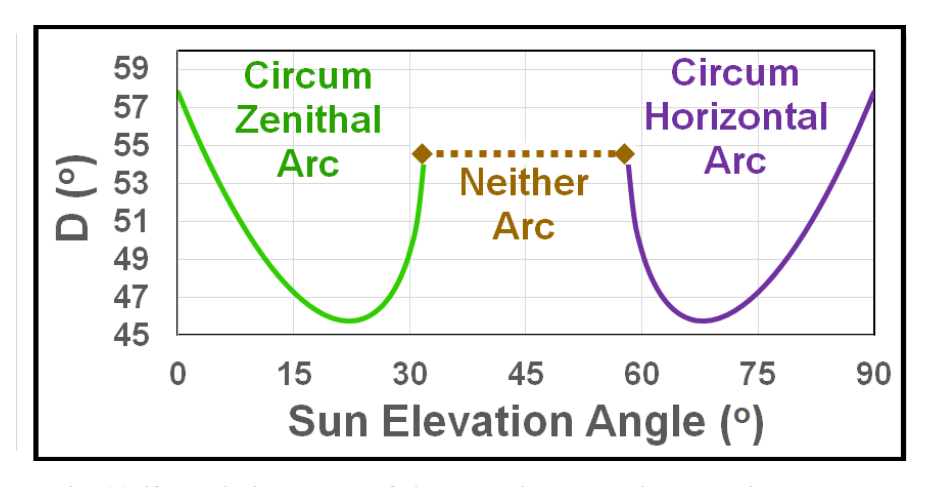


Fig. 11-43. Deviation angles of circumzenithal and circumhorizontal arcs as a function of  $H_{\rm SUN}$ . SDG.

Both the CZ and the circumhorizontal (CH) arcs vary with  $H_{\rm SUN}$  (Fig. 11-43). The CZ arc forms when sunbeams enter the top hexagonal end face and exit a vertical rectangular side, but it can only form when  $H_{\rm SUN} <\approx 32^{\rm o}$ . It is brightest, most spectral and comes nearest the Sun (46°) when  $H_{\rm SUN} \approx 22^{\rm o}$ . The CH arc is its complement in almost every way. The CH arc only occurs when  $Z_{\rm SUN} <\approx 32^{\rm o}$  and is brightest, nearest the Sun and most spectral when  $Z_{\rm SUN} \approx 22^{\rm o}$ . It is, however almost never seen with the parhelia, which disappear once  $Z_{\rm SUN} < 29^{\rm o}$ .

As with the parhelia, the intensity of the CZ and CH arcs vary with  $H_{SUN}$  (Fig. 11-44). Also, as with the parhelia, the intensity of the CH and CZ arcs depends on the crystal aspect ratio, thin plates producing brighter

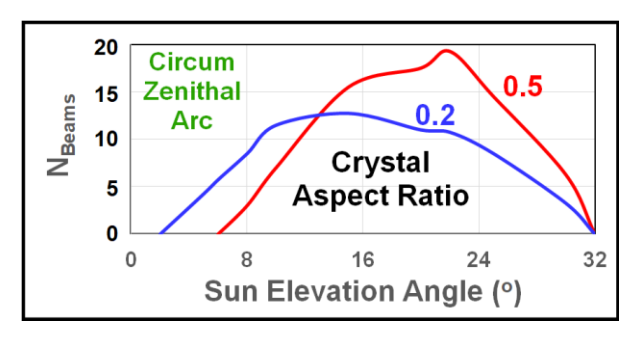


Fig. 11-44. Relative brightness of the circumzenithal arc as a function of HSUN for two values of crystal aspect ratio. SDG.

CZ arcs when the Sun is low in the sky and thicker plates producing brighter CZ arcs when the Sun is higher in the sky.

#### 3: Halo Color and Width

The greater spectral color purity of the arcs associated with the 46° halo is due in good part to their greater width than the arcs of the 22° halo. For example, the CZ and CH arcs are 1.57° wide at their maximum spectral purity, while the Parry arc is only 0.76° wide. These angular widths must be compared to the Sun's angular width (0.53°), which smudges and blurs (similar to an astigmatism) all rainbows and halos and reduces their color purity. The wider the halo arc and the greater the angular spread of the spectrum, the smaller the relative role of the Sun's smudging and therefore the smaller the reduction of spectral purity.

When comparing spectral purity of rainbows and halos, rainbows, have two advantages, while the CZ and CH arcs at their optimal Sun angles have one. Rainbows form in the rain shafts under thick clouds with potentially dark backgrounds while most halos form with sunlit skies as their background. Recall how adding to background lighting detracts from rainbow appearance in Fig. 9-5.

Celestial (above horizon) halos must also pass through the ice crystal clouds they are produced in. Once the optical thickness of the cloud exceeds about 5, virtually all halos disappear. Rainbow spectra also suffer as the optical thickness of the rain shaft increases, but because

they are reflected in the raindrops and do not have to penetrate the rain shaft, they remain visible for much larger values of optical thickness. The same is also true for 'infernal' halos emerging from the clouds below, and they will stand out best when the surface below is dark, as it is over the ocean.

The high color purity of the CZ and CH arcs at their optimal Sun angles occurs because all rays are deflected by  $D_{\min}$ , which varies only by wavelength. This is also true of the Parry halo when the Sun is at the zenith (an extremely rare event).



Fig. 11-45. Halo complex in morning ice fog Hörnli Arosa Switzerland 30 Nov 2019 with  $T = -7^{\circ}\text{C}$ , ©Michael Schneider

# 11.7 Complex Halo Displays

Complex halo displays are among the atmosphere's most awesome, sights. They cross the sky with multiple halo forms that usually appear alone or in much smaller combinations, and often include rare

halos. The brilliance, colors, and sculpted geometric forms that appear in thin air rivet attention from casual observers as well as halo experts.

The uninitiated may experience a sense of bewilderment, and ask, "What could possibly cause such a complex apparition in thin air?" The answer is simpler than the complex appearance. Since each halo form is produced by a specific crystal form and orientation at specific Sun elevation angles halo complexes must be produced in clouds or ice fogs that contain several distinct crystal forms and orientations, and little junk ice when the complexes are brilliant and contain rare halos.

Connecting displays with crystals we find first that the brilliant bur relatively simple display of Fig. 11-15 involved two crystal forms and orientations. Horizontal plates produced the parhelic circle and the CH arc since the Sun was high ( $H_{SUN} \approx 72^{\circ}$ ) and nearly horizontal pencils produced the circumscribed halo that might be mistaken as a 22° halo. The display of Fig. 11-17 required tumbling prisms (possibly thick plates) to produce the 22° halo and since it occurred with  $H_{SUN} \approx 22^{\circ}$ , horizontal plates produced parhelia just outside the halo and a brilliant spectral CZ arc. It also required a small percentage of horizontal pencils to produce the weak upper tangent arc and faint supralateral arcs.

The more complex display of Fig. 11-1 not only required the abovementioned crystals (with a much larger percentage of horizontal pencils), but also a significant fraction of Parry-oriented pencils (rectangular prism face horizontal) to produce the upper) suncave Parry arc, the hook-like Tape arcs on the supralateral and infralateral arcs, and the heliac arc.

Brilliant displays also require very constrained weather and cloud conditions. The conditions that led to the complex of Fig. 11-1 were documented by Claudia Hinz, who maintained and practically lived on the Deutscher Wetterdienst's meteorological observatory atop Mount Fichtelberg in Germany's Ore Mountains for more than a decade and never (well, almost never) missed an opportunity to

photograph beautiful scenes. On the morning of 31 Jan 2014, there was a pronounced temperature inversion with a gentle but insistent wind that forced humid, cold air layer from the valley to ascend the modest peak, and cool even more as it rose. At T = -8°C and low supersaturation, the Nakaya diagram (Fig. 11-25) shows that both solid plate and solid pencil crystals form.

That makes it no coincidence that the halo complex photographed by Michael Schneider on another ski slope (Fig. 11-45), which closely resembles that of Fig. 11-1 occurred in a thin ice fog at  $T = -7^{\circ}$ C.



Fig. 11-46. South Pole Halo Display of 11 Jan 1999. Marko Riikonen

Most of the most magnificent displays contain sparkling diamond dust and blue skies, as in the South Pole display of 11 Jan 1999 photographed by Marko Riikonen (Fig. 11-46), showing they form in thin ice fogs right at ground level. Geometry demandss that an object that spreads over a large angle of the visual field be small if it is close and large if it is far. It is much more likely for a nearby ice fog that a viewer is immersed in to contain a narrow range of near perfect crystals than for a distant cirrostratus cloud high above the ground in the upper troposphere. Furthermore, most cirrostratus cloud extend

over a wide range of heights and temperatures in storms with embedded convection, which makes it unlikely in the extreme to consist almost entirely of simple crystal forms with no junk ice.

In the case of diamond dust halos it is possible to collect the crystals responsible for a halo complex as they fall to the ground, though it is a difficult task because crystals change rapidly when atmospheric conditions change. When Robert Greenler and Walter Tape and Marko Riikonen and others went to the South Pole in search of complex halo displays, which form near the surface of the ice cap, they collected and photographed the delicate crystals, which change so rapidly on being collected a crystal census can only be indicative. However, even an accurate crystal census only suggests their orientations in the air.

When crystals producing a complex halo display cannot be collected and their fall mode only surmised, we hve already shown that detective work involving trial and error with computer simulations are needed to solve the mystery of the mix of crystals forms and orientations needed to produce halo complexes. Computer simulations of halos answer many questions because they can produce astoundingly photorealistic halos. They start by using the known connections between each halo form and the likely crystal forms and orientations and then vary the fractions of each crystal form and orientation until the simulated halo display matches photographs of the actual display. And though some uncertainty may remain, the matches can be impressive.

Table 11-3. Crystals for simulations of Fig. 11-42.

`Form	%	Aspect	C-Axis	Tilt (°)	Other
		Ratio	Oriented		
Plate	20	1	Rnd		
Pencil	50	5	Vert	2	
Pencil	10	5	Vert	2	Parry Tilt = 1°
		And eitl	her		·
Plate	20	0.3	Horiz	2	
Pyrmd	20	0.2	Horiz	2	Pyr Aspect Ratio = 0.2

The mix of crystal forms and orientations used to produce the simulation (Fig. 11-42) of the halo complex of Fig. 11-39 is given in Table 11-3. As pointed out, this mix was the result of many computer runs and adjustments that were made to produce the suncave Parry arc and to capture the relative brightness and color of the various halos. For example, to make the upper tangent arc suitably brighter than the sunvex Parry arc required at least five times as many horizontal pencils with random spin about the c-axis than with the Parry orientation of a rectangular face near horizontal.

### 11.8 Halos and Optical Thickness

Perfect ice crystal prisms and pyramids focus light to such a degree that halo spots and arcs (recall Table 11-2) sometimes appear in clouds that are invisible to the naked eye and do not impair the sky's pristine blue. Sometimes, sparkling diamond dust is the only giveaway that any ice crystals at all are present. Junk ice, which dominates thunderstorm anvils and is a significant fraction in most cirrostratus ejected from cyclones, impose the main limitation on the brightness of halos, rendering them feeble or eliminating them.

The cloud's optical thickness,  $\tau_{\text{CLD}}$  is the second major factor limiting halo brightness. Recall from §2.4 that the fraction of light that penetrates a cloud or a volume of air depends on its optical thickness,  $\tau$ , and is given by the fraction,  $e^{-\tau}$ . This is illustrated by the solid curve in Fig. 11-47. In optically thin clouds (e. g.,  $\tau \leq 0.1$ ), most sunlight passes through without being scattered, but as  $\tau$  increases the fraction that passes through undisturbed diminishes so rapidly that at  $\tau = 5$  only 0.67% of the initial beam gets through undisturbed, and most of the initial sunlight has been scattered two or more times.

Halos are produced by sunbeams that have been scattered once and only once. Light scattered two or more times is almost invariably incoherent and contributes to the background skylight. In optically thin clouds (e. g.,  $\tau \le 0.1$ ) most of the small fraction of scattered

light is scattered only once, and if that light is focused on a small region of the sky it may produce a bright halo. Singly scattered light peaks at  $\tau = 1$ , but the fraction of multiply scattered light is already significant.

In optically thick clouds, very little sunlight passes through the cloud without being scattered, and most is scattered more than once. For example, at  $\tau_{\text{CLD}} = 2.5$ , 92% of the light has been scattered, but only 20% has been scattered once. At  $\tau_{\text{CLD}} = 5$ , 99.33% of the light has been scattered, but only 3.6% has been scattered once. Thus, as  $\tau_{\text{CLD}}$  increases, the fraction of background light increases while the fraction of singly scattered light that could produce a halo decreases.

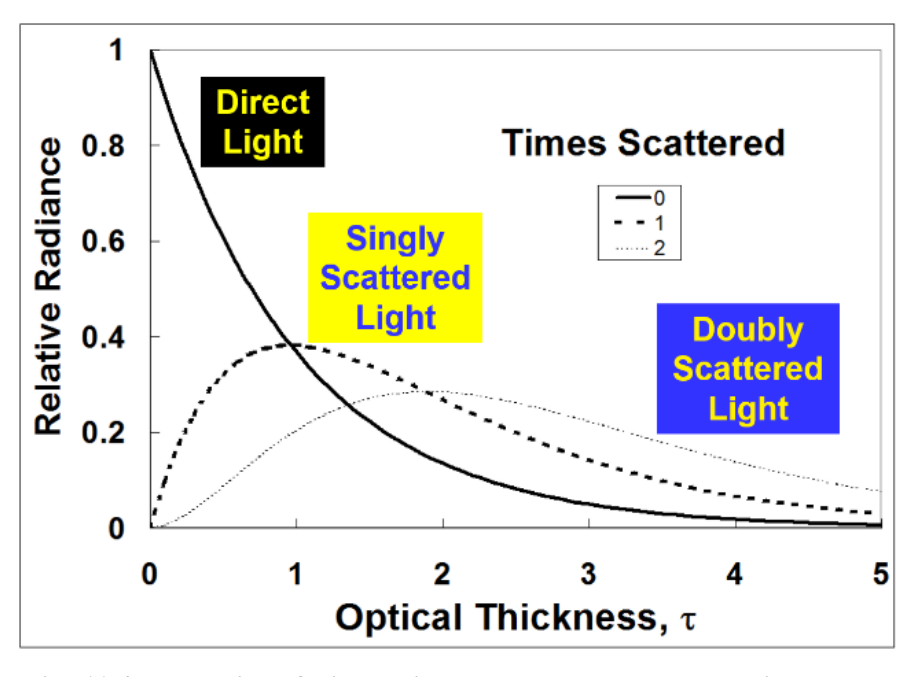


Fig. 11-47. Intensity of direct, singly, and doubly scattered light as a function of optical thickness,  $\tau$ . SDG.

The simulations of Fig. 11-48 were run for  $H_{SUN} = 25^{\circ}$  in a slightly hazy atmosphere where aerosols add 20% to the optical thickness of the clear air. The 22° halo made by perfect thick, solid, randomly oriented plate crystals is bright when  $\tau_{CLD} \approx 0.01$  (implying that the

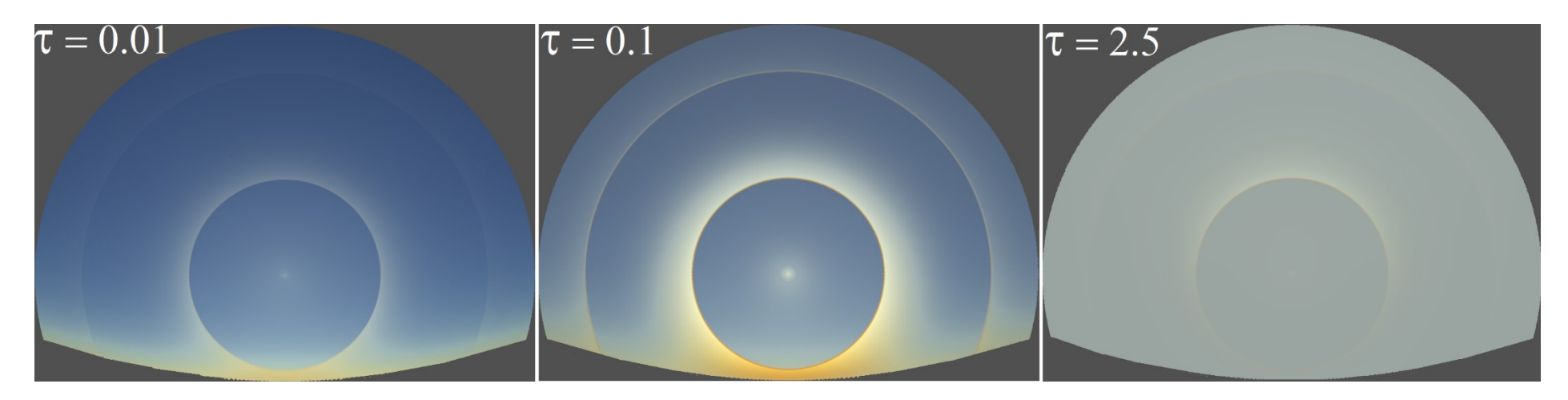


Fig. 11-48. Simulations of halo and sky brightness and color as a function of cloud optical depth ( $\tau_{cld}$ ) for  $H_{SUN} = 25^{\circ}$  and thick plate crystals in a cloud at p = 300 hPa.

potentially brighter halo forms can appear bright at cloud optical depths,  $\tau_{\rm CLD} < 0.001$ ). At  $\tau_{\rm CLD} \approx 0.1$ , the 22° halo is brilliant, and even the 46° halo is distinct, and while the sky has lost some of its pristine brilliance, it is still deep blue except near the horizon.

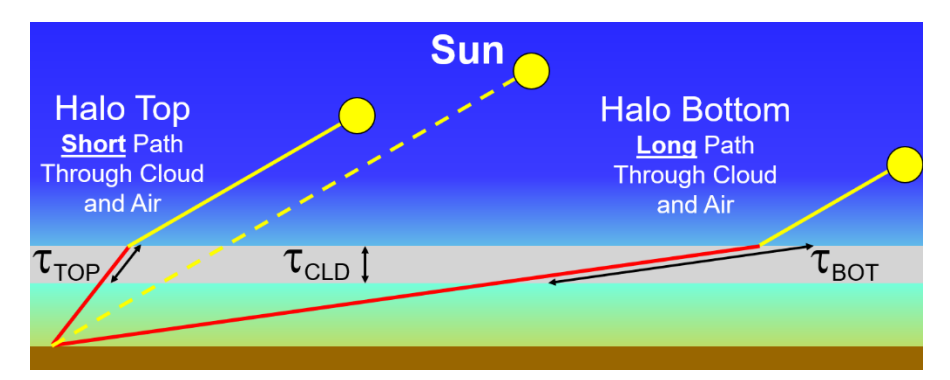


Fig. 11-49. Optical paths of halo top and bottom for a high cloud layer. When the Sun is low in the sky,  $\tau_{\rm BOT} >> \tau_{\rm TOP}$  and halo bottoms tend to be faint.

Halos have the greatest contrast with the background sky in the range  $0.2 < \tau_{\rm CLD} < 0.5$ . As  $\tau_{\rm CLD}$  continues to increase background sky and cloud light increase more rapidly than the halo beam. The right panel of Fig. 11-47 shows that at  $\tau_{\rm CLD} = 2.5$ , the sky is gray, the entire  $46^{\circ}$  halo and the bottom of the  $22^{\circ}$  halo have vanished, and the top of the  $22^{\circ}$  halo is feeble. This unexciting view, with is quite common when

the Sun is low in the sky and cirrostratus clouds are thick enough to turn the sky gray.

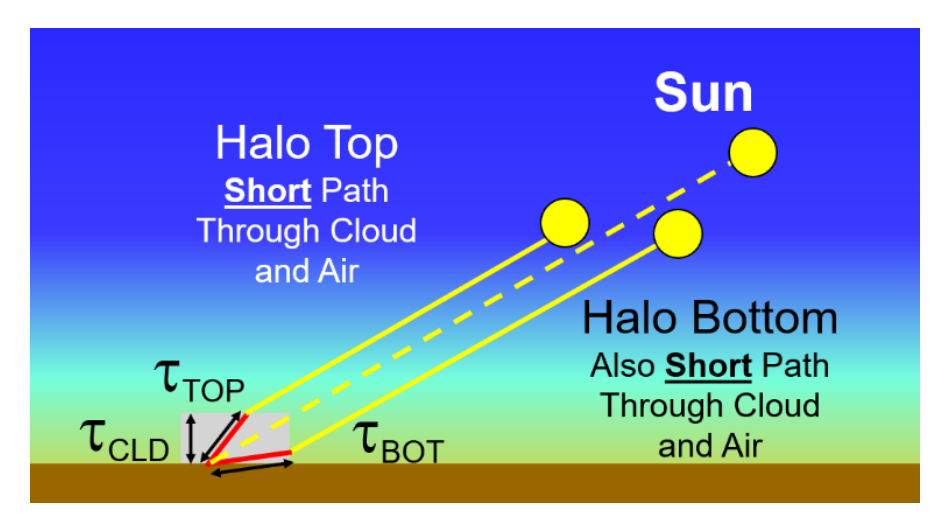


Fig. 11-50. Optical paths of halo top and bottom for a cloud at ground level.

Fig. 11-49 illustrates why halos produced in cirrostratus clouds that cover the sky from end to end in a layer fade near the horizon. Light arriving from the bottom of the halo must pass so obliquely through a high cloud layer that its path both through the cloud and the atmosphere below, is very long. If the optical depth of the cloud for a vertical sunbeam,  $\tau_{CLD} \approx 2.5$ , then when  $H_{SUN} = 25^{\circ}$ , the optical

thickness a beam at the bottom of the halo (at  $H_{\rm OBS} \approx 3^{\circ}$ ) must pass through,  $\tau_{\rm BOT} \approx (19.1 \times 2.5)$  is so large that no direct sunlight or singly scattered (halo) light can penetrate such a cloud.

By contrast, diamond dust halos, which are usually produced by tenuous clouds or fogs of limited width (as opposed to extensive layers) near the ground can be blindingly bright in almost pristine skies because the optical thickness of the path through the cloud and air is small (Fig. 11-50).

### 11.9 Simulating Halos (Photorealism)

Where nature is stingy, we can be generous.

It is a joy to create photorealistic simulations of halos and other optical phenomena. They are done using the same techniques used to create photorealistic computer images of any scene in modern animated films. And they can be done for any imagined crystal forms and tilts, all ideal if desired.

The starting point for simulations of atmospheric optical phenomena is to apply the appropriate laws of scattering to a single particle. For example, the Lee diagram for rainbows and cloudbows (recall Fig. 9-31) was produced using Mie scattering for spherical water drops of a range of sizes. The angular distribution of the relative scattering intensity for raindrops, randomly oriented thick ice crystal plates, cloud droplets ( $r_D = 6 \mu m$ ) and air molecules was shown in Fig. 2-4.

The next step is to let the particles scatter sunbeams around the sky. Sunbeams are aimed at random spots on a drop for a rainbow or an ice crystal for a halo, and air molecules and aerosol particles are included as scatterers in proportion to their optical thickness. In the perfect, single scattering, Monte Carlo dot model (the simplest of the models), the instant beams are scattered they are plotted as dots on the computer screen. In the early models, the dots were black; now they are colored in proportion to the solar spectrum.

The perfect, single scattering model gives a good idea of the shape and maximum possible brightness and greatest color purity of the phenomena, but it rejects any chance that the scattered beam can itself be scattered again and removed from the rainbow beam or halo beam in its voyage through the atmosphere and cloud.

The next order of approximation in the heirarchy of models is to include the probability that a beam will be scattered again before reaching the observer, and remove the beams that are scattered a second time. That level of model gives an excellent approximation to halos and rainbows that appear in or through optically thin clouds. There are even good analytic mathematical formulas for such models provided the ice crystals tumble randomly, so dots are not necessary, and the halos depicted approach photorealism as in Fig. 11-42, but only for circular halos.

The most accurate model, of course, must allow each beam to be scattered as many times as necessary until it reaches the observer or is extinguished, or is scattered back out to space (where it can be seen as an infernal halo.

Photorealistic halo simulations with real sky backgrounds can be made with a six-layer, Monte Carlo multiple scattering model (Fig. 11-51). Sunbeams first pass through Layer 1, the ozone layer. The best-known impact of Ozone is to protect life on Earth by absorbing ultraviolet light. Its lesser known impact on atmospheric optics is to make the sky bluer by preferentially absorbing orange and red light in the so-called Chappuis bands ( $\lambda \approx 0.605 \,\mu m$ ).

Layer 2 is the clear air above cloud top. Rayleigh scattering is the sole process. Elevated aerosol layers certainly do occur in the atmosphere but were not considered important for most bright halos.

Layer 3 is the cloud layer, where ice crystals of chosen form, orientation, and optical depth scatter light. This is the most time consuming part of the model, especially when the cloud's optical depth,  $\tau_{\rm CLD} >> 0.1$ . Fortunately, for the purposes of computer time, almost all the best halo displays occur for small values of  $\tau_{\rm CLD}$ .

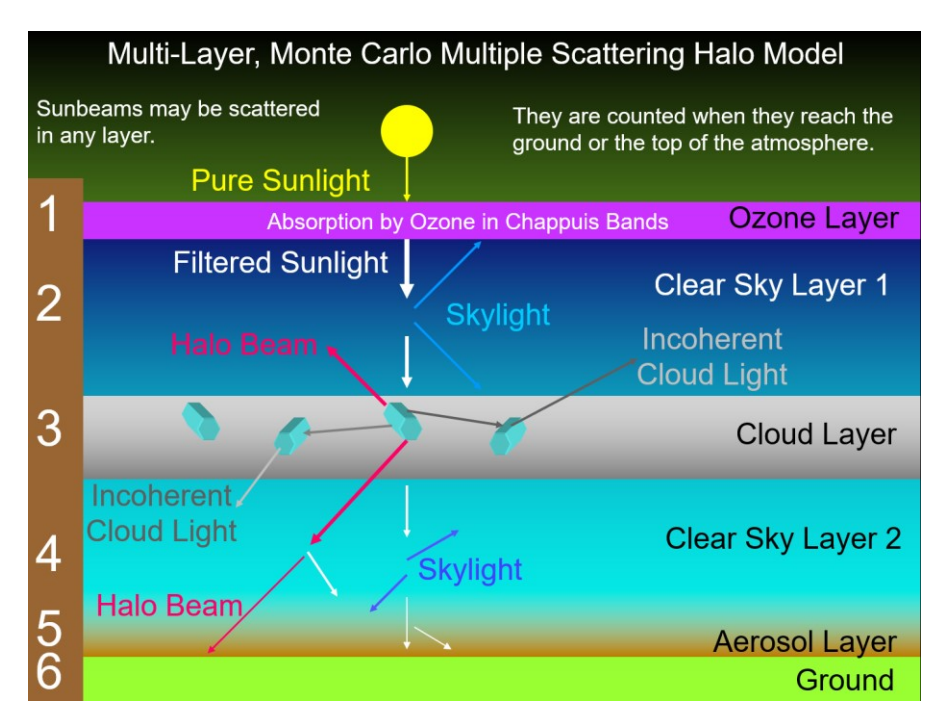


Fig. 11-51. Six-layer halo model including cloud and atmosphere. SDG.

If the cloud layer occurs above the atmospheric boundary layer, Rayleigh scattering occurs beneath cloud base in Layer 4. Layer 5, the aerosol layer is placed just above the surface since under normal conditions most aerosols are confined near ground level. Layer 6 is the ground, which can impact background sky lighting by reflecting light. This is important over snow-covered ground.

In this six-layer model, sunbeams of 61 wavelengths distributed over the visible light range in proportion to the Planck radiation curve usually set at T = 5750 and reduced by ozone absorption are 'shot' into the atmosphere and are plotted as dots and recorded in files after they reach the ground (albedo is usually neglected) or the level of an observer in a jet if the model is set to plot infernal halos.

The dot models give a good idea of the potential shape and color of the phenomena but are not photorealistic. The computer monitor is the chief limitation. In the regions of the sky, such as where the parhelia are located, the monitor quickly becomes saturated with dots and cannot become any brighter while other parts of the sky have no dots at all.

The problem of excess dots is solved by dividing the sky into tiny squares or pixels and recording the dots of each color in each pixel. Separate files are made for 1: halo dots that have struck ice crystals once or twice without striking an air molecule or aerosol particle, and, 2: sky dots, which include all other scattered dots. Dots of direct sunlight that reach the ground without being scattered are not recorded as too bright.

The sky dots are so sparse that to approach photorealism requires at least 10 million dots at each wavelength or computer time of several hours on a fast PC. Even then, random variations from one pixel to the next are large enough to make the sky appear spotty. That problem is reduced smoothing, which amounts to averaging nearby pixels.

Smoothing is not applied to the halo dots because 1: their number in each pixel is large enough so that smoothing is not necessary and, 2: smoothing broadens the narrow halos unrealistically but has much less impact on the broad, slowly changing background sky except right above the horizon and immediately around the Sun.

The smoothed sky dots in each pixel are then added to the halo dots and all pixels are illuminated on the monitor in proportion to the brightest pixel to produce the final image. Similar techniques have been used to create the frames for animated movies.

The difference between the dot model and the final halo simulation can be seen by comparing Fig. 11-52 to Fig. 11-4. These represent different views of a highly idealized halo situation designed to bring out a large number of halo forms and not match any particular halo complex though it does contain many of the halos seen in the complexes of Fig. 11-1, Fig. 11-45 and Fig. 11-46. Very stringent limits, indicated in Table 11-4 were placed on the crystals. All were perfect prisms, and the tilt of the aligned crystals had almost no variation. The simulation was produced for  $H_{SUN} = 30^{\circ}$  to make the

lower tangent arc visible without having to look downslope as in Fig. 11-1, and many of the arcs linked to the 46° halo to be near optimum.

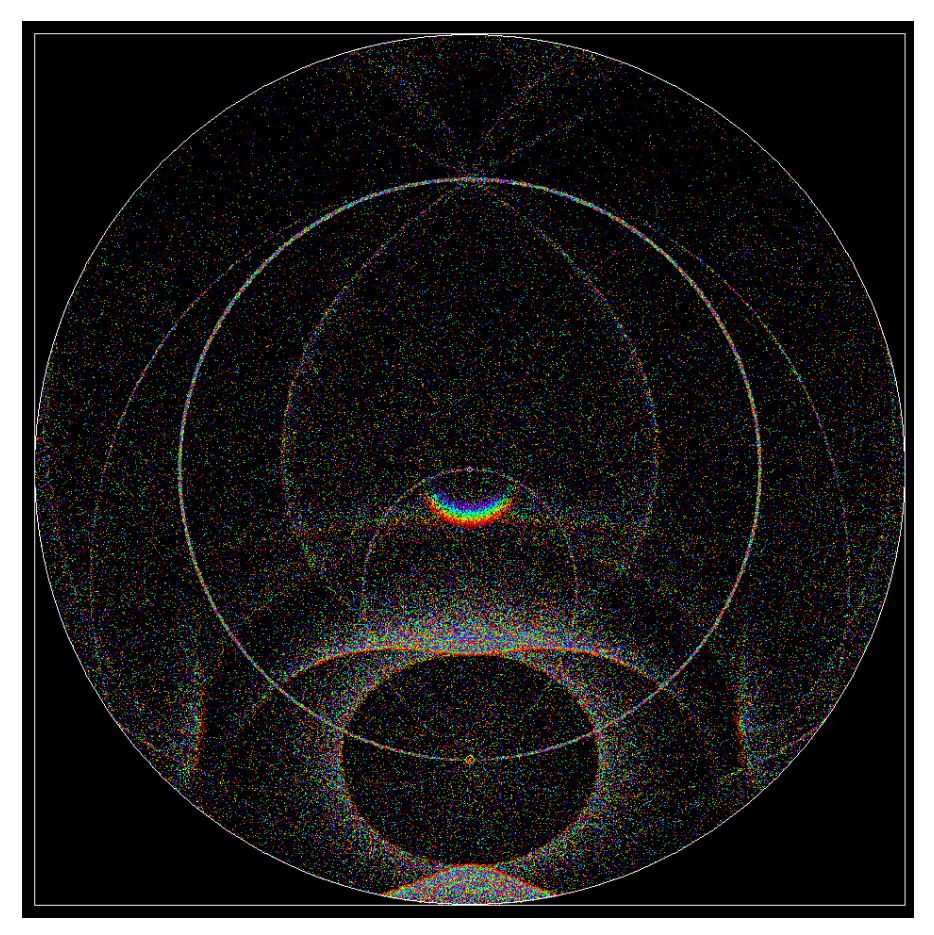


Fig. 11-52. All sky dot model version of the halo complex simulation of Fig. 11-4. SDG.

Table 11-4. Crystal Properties for Simulation of Halo Complex if Fig. 11-4.

Crystal % 20%	Fall Mode Random	Aspect Ratio 1.0	Tilt (°) 0 - 90
30%	C-axis vertical	0.3	0 - 0.1
30% 45%	C-axis horizonta	1 3.0	0 - 0.1
05%	Parry	3.0	0 - 0.1

The dot model of Fig. 11-52 shows most of the arcs with only 10,000 dots per wavelength, whereas the near photorealistic simulation of

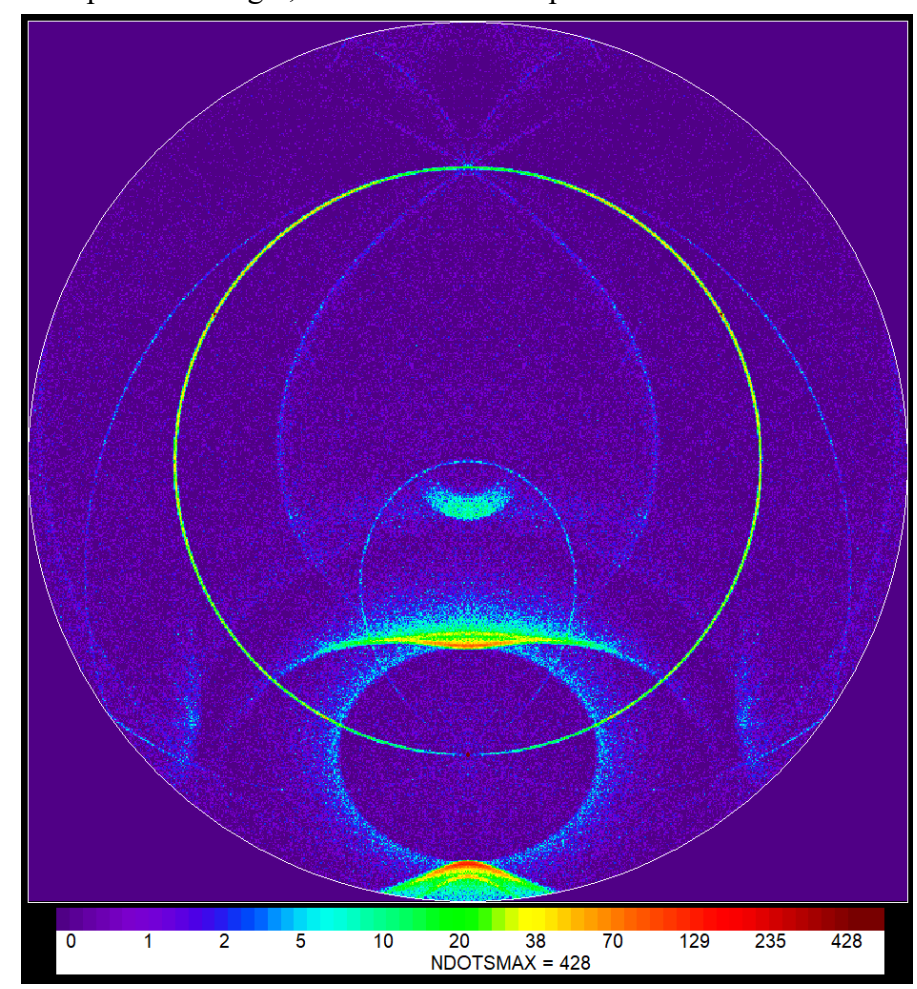


Fig. 11-53. False color image of dot density of dot model of Fig. 11-51. SDG.

Fig. 11-4 required 10 million dots per wavelength, The dot model fails to show the parhelia because the tilt of the plate crystals is so small the parhelia are little more than dots immersed in the parhelic circle. The false color dot density map of Fig. 11-53 gives a better idea of the relative brightness of the halo forms, but does require a close look to see the existence of the parhelia. It also highlights the lower Parry arc, which is easily missed in both Fig. 11-4 and Fig. 11-51.

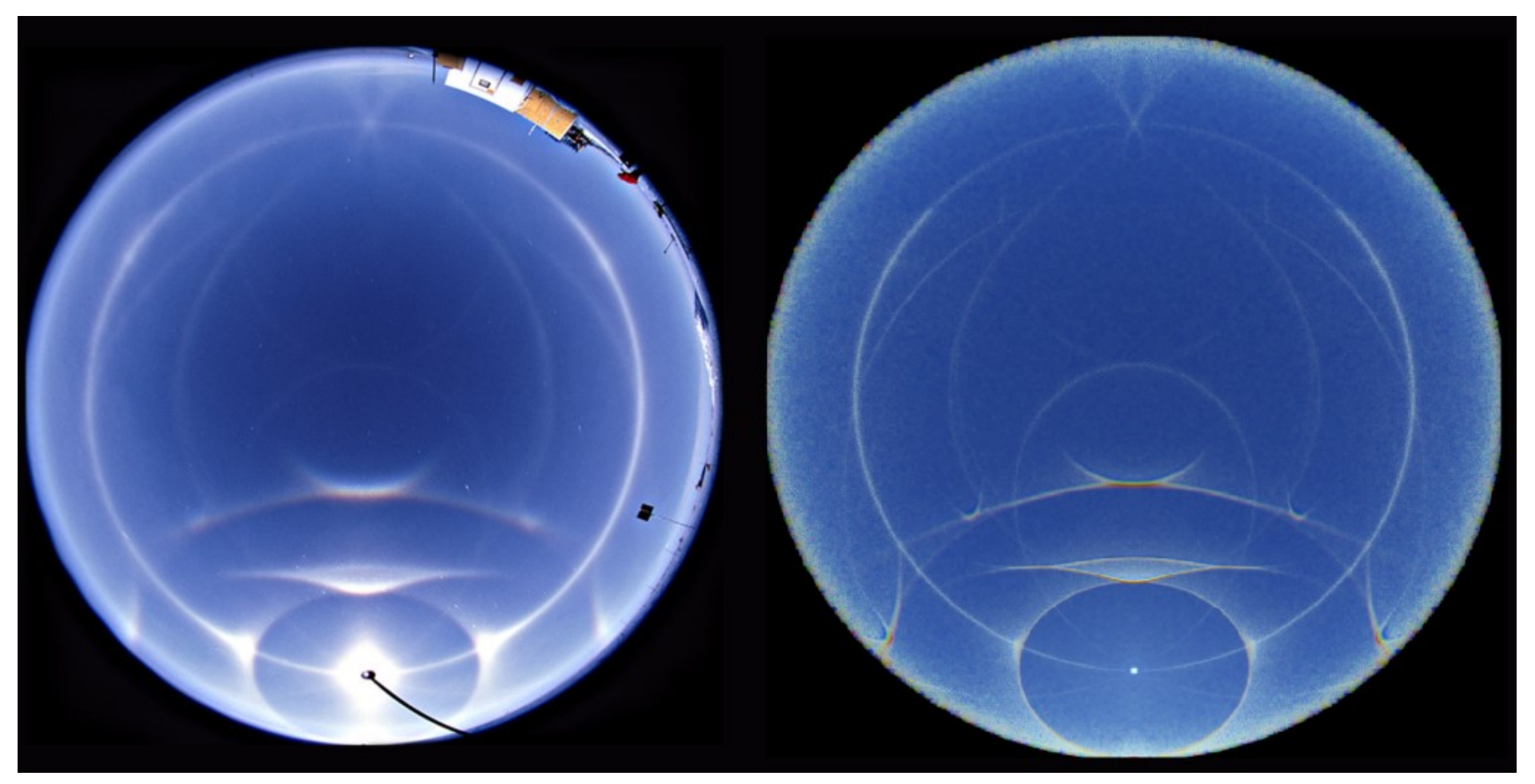


Fig. 11-54. Fisheye view of South Pole Halo Display of 11 Jan 1999. Sun and several bright arcs are broadened by overexposure. ©Marko Riikonen.

Table 11-5. Crystal Properties for Simulation of South Pole Halo Display of 11 Jan 1999.

Crystal %	Fall Mode	Aspect Ratio	Tilt (°)
Crystal % 30%	Random	1.0	0 - 90
22.5%	C-axis vertical	0.3	0 - 5
40%	C-axis horizontal	3.0	0 - 2
7.5%	Parry	3.0	0 - 2

It is appropriate to conclude this chapter by comparing halo complexes with simulations. The South Pole Halo display of 11 Jan

Fig. 11-55. Simulation of South Pole Halo Display of 11 Jan 1999.

1999 (Fig. 11-54), photographed by Marko Riikonen, was a magnificent complex halo display with arcs that traversed the entire sky. Fig. 11-46 is an all-sky, or fisheye view, where the zenith is at the center and the circumference represents the horizon. This is shown side-by-side with the simulation of the complex using the 6-layer model with up to 10 million beams (Fig. 11-55). Atmospheric conditions used in the model include surface pressure,  $p_{\rm sfc} = 700$  hPa, atmospheric turbidity = 1.05 with aerosols of radius,  $r_{\rm AER} = 0.3$  µm, and the ice crystal cloud at the surface with optical depth,  $\tau_{\rm CLD} =$ 

0.05 and 10% junk crystals. The halo-producing ice crystals, their relative abundance and properties are listed in Table 11.5.

The simulation captures the major features of the display though it makes the halos too narrow and colorful and makes the parhelic circle too faint. These discrepancies can be reduced by increasing the maximum tilts of the crystals, and the percentage of oriented plate crystals. Furthermore, the simulated sky near the horizon remains spotty. That problem can be reduced by either increasing the number of beams or by an improved method of smoothing. The photo itself is also an imperfect copy of the real halos, largely because it suffers from the unavoidable overexposure of the Sun and of the brightest halos, which causes both bleaching of the colors and unrealistic broadening.

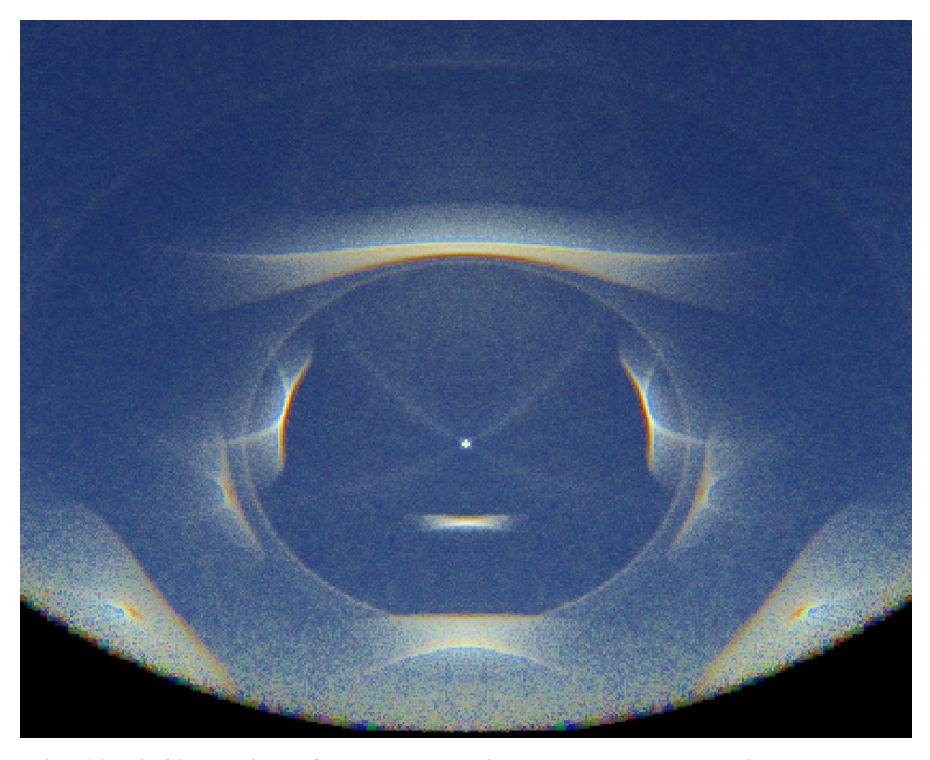


Fig. 11-56. Simulation of Lunar halo display produced by oriented stunted bipyramidal crystals of 06 Jan 2004. SDG.

Finally, Fig. 11-56 represents a simulation of the halo display over Fairbanks, AK at 4:19 AM on 06 Jan 2004 photographed by Walt Tape (Fig. 15.11, *Atmospheric Halos and the Search for Angle x*) when the Moon's elevation  $H_{LUN} = 35^{\circ}$ . The simulation used 80% stunted bipyramids with the c-axis tilted up to 15° and included for the purpose of reference 20% tumbling thick plates (that were not in the actual display. Cloud optical thickness was set to,  $\tau_{CLD} = 0.05$  in a pure molecular atmosphere. The simulated arcs closely match the real arcs and though they are far more distinct and narrow than the photo, they do indicate what is possible for perfect crystals in a perfect atmosphere.

Considering how seldom the atmosphere provides extraordinary halo displays, especially where most of humankind lives, and ignoring the discrepancies between reality and artifice, simulating halos is a rewarding substitute while wishing and waiting for the real thing.



Fig. 11-56. Sun pillar facing NW at twilight forming below altocumulus at 8200 m and T = -26°C, San Mateo, CA 28 Jun 2015 . SDG.